

Review

# Human Cartilage Biomechanics: Experimental and Theoretical Approaches towards the Identification of Mechanical Properties in Healthy and Osteoarthritic Conditions

Elisa Belluzzi <sup>1,2,3</sup> , Silvia Todros <sup>3,4,\*</sup> , Assunta Pozzuoli <sup>1,2,3</sup> , Pietro Ruggieri <sup>2,3</sup> ,  
Emanuele Luigi Carniel <sup>3,4</sup>  and Alice Berardo <sup>3,5,6</sup> 

- <sup>1</sup> Musculoskeletal Pathology and Oncology Laboratory, Department of Surgery, Oncology and Gastroenterology, DiSCOG, University of Padova, 35128 Padova, Italy; elisa.belluzzi@unipd.it (E.B.); assunta.pozzuoli@unipd.it (A.P.)
- <sup>2</sup> Orthopedics and Orthopedic Oncology, DiSCOG, University of Padova, 35128 Padova, Italy; pietro.ruggieri@unipd.it
- <sup>3</sup> Centre for Mechanics of Biological Materials, University of Padova, 35131 Padova, Italy; emanueleluigi.carniel@unipd.it (E.L.C.); alice.berardo@unipd.it (A.B.)
- <sup>4</sup> Department of Industrial Engineering, University of Padova, 35131 Padova, Italy
- <sup>5</sup> Department of Civil, Environmental and Architectural Engineering, University of Padova, 35131 Padova, Italy
- <sup>6</sup> Department of Biomedical Sciences, University of Padova, 35131 Padova, Italy
- \* Correspondence: silvia.todros@unipd.it; Tel.: +39-049-827-6878

**Abstract:** Articular cartilage is a complex connective tissue with the fundamental functions of load bearing, shock absorption and lubrication in joints. However, traumatic events, aging and degenerative pathologies may affect its structural integrity and function, causing pain and long-term disability. Osteoarthritis represents a health issue, which concerns an increasing number of people worldwide. Moreover, it has been observed that this pathology also affects the mechanical behavior of the articular cartilage. To better understand this correlation, the here proposed review analyzes the physiological aspects that influence cartilage microstructure and biomechanics, with a special focus on the pathological changes caused by osteoarthritis. Particularly, the experimental data on human articular cartilage are presented with reference to different techniques adopted for mechanical testing and the related theoretical mechanical models usually applied to articular cartilage are briefly discussed.

**Keywords:** cartilage; biomechanics; osteoarthritis; experimental tests; constitutive modeling



**Citation:** Belluzzi, E.; Todros, S.; Pozzuoli, A.; Ruggieri, P.; Carniel, E.L.; Berardo, A. Human Cartilage Biomechanics: Experimental and Theoretical Approaches towards the Identification of Mechanical Properties in Healthy and Osteoarthritic Conditions. *Processes* **2023**, *11*, 1014. <https://doi.org/10.3390/pr11041014>

Academic Editor: Bonglee Kim

Received: 9 February 2023

Revised: 24 March 2023

Accepted: 25 March 2023

Published: 27 March 2023



**Copyright:** © 2023 by the authors. Licensee MDPI, Basel, Switzerland. This article is an open access article distributed under the terms and conditions of the Creative Commons Attribution (CC BY) license (<https://creativecommons.org/licenses/by/4.0/>).

## 1. Introduction

Articular cartilage (AC) is a complex connective tissue, mainly composed of hyaline cartilage, which plays a key role for load bearing, shock absorption and lubrication for joints throughout the body, providing a low friction coefficient [1]. AC experiences a variety of applied loads, such as compression, shear, friction and tension. It is extremely strong (strength 9–40 MPa), tough (fracture energy 1000–15,000 J m<sup>-2</sup>) and presents a high strain at break (strain 60–120%) [2].

However, traumatic events, aging, degenerative pathologies and other comorbidities (such as obesity) may affect the structural integrity of AC through the years, causing pain and long-term disability [3–6].

Among the musculoskeletal diseases, osteoarthritis (OA) represents a health issue, which concerns 1 out of 4 people in Europe, rating as one of the most common pathologies worldwide [7]. Moreover, due to the avascular and abneural nature of AC, its healing capacity after damage is strongly limited and the effects of OA have a degenerative impact [8].

It has been observed that this disease has non negligible reflexes also on the mechanical behavior of AC [9–11]. From a biomechanical point of view, pathological AC exhibits an

average decrease in its layer thickness and mechanical properties such as stiffness, with respect to healthy cartilage. On the contrary, it is characterized by a higher permeability, which regulates both tribological and bearing activities, and its changes are also correlated to the OA grade [10,12].

The mechanical properties of healthy and pathological AC and the main factors influencing the mechanical response to applied loads represent fundamental features to be known in order to pursue not only the recovery, but also the regeneration of new functional tissue [13]. Indeed, the mechanical behavior of regenerated AC should mimic the one of native tissue as closely as possible, in terms of compressive elastic and viscoelastic behavior, but also with regard to tribological properties [14]. Several biomaterials have been tested as articular substitutes, including natural (i.e., collagen, hyaluronic acid, chitosan, silk fibroin, gelatin) and synthetic (polycaprolactone, polylactic-co-glycolic acid, poly(L-lactic acid), polyurethane) polymers [15–18]. In addition, Poly(Vinyl Alcohol) (PVA) hydrogels have been extensively investigated and applied for the repair of cartilage defects *in vitro* or *in vivo*, due to their hydrophilic nature, good biocompatibility and suitable mechanical strength [19,20]. However, there is still the need to improve the mechanical behavior of these materials, to match that of native AC. To this intent, the here proposed review reports a brief description of the experimental techniques currently used to characterize the mechanical properties of human AC and the related theoretical models usually applied for its mechanical description. Then, particular attention is paid to the physiological aspects that influence AC microstructure and biomechanics, such as aging, and a special focus has been addressed to quantify the pathological changes caused by the OA to mechanical properties of AC. Additionally, mechanical results obtained from animal samples have been reported, since they are frequently used as a model system for human cartilage thanks to the easier tissue availability, even if differences in shape, size, biochemical content and matrix architecture influence the final correlation with respect to human cartilage.

All these insights could be useful to summarize the main biomechanical properties of AC and how these results have been obtained, as a comparison with future studies on artificial AC.

## 2. Articular Cartilage

AC is a specialized type of hyaline cartilage, which is the most abundant type of cartilage in the body, and it is 2–4 mm thick [21]. AC is composed by 60–80% of water (by wet weight), collagen II (15–22% by wet weight), chondrocytes (5–10% of tissue volume), proteoglycans (PGs) (4–7% by wet weight), minerals (<4%) and matrix proteins (<1%) [22]. Importantly, AC is an avascular tissue and does not have nerves or lymphatics [23].

AC can be described as a porous, viscoelastic material consisting of three principal phases: solid extracellular matrix (ECM) phase, a fluid phase of water (interstitial fluid) and an ion phase (composed by dissolved electrolytes with negative and positive charges, <1% [24]). These phases give to the tissue the ability to withstand compressive loads [24].

AC is an anisotropic tissue composed by 4 zones: the superficial (or tangential) zone (10% to 20% of AC thickness), the middle (or transitional) zone (40% to 60% of the total cartilage volume), the deep (or radial) zone (approximately 30% of AC volume) and the calcified zone (Figure 1).

Three regions can be observed in each zone: the pericellular matrix (PCM), the territorial matrix (TM) and the interterritorial matrix (ITM). AC composition and structure are fundamental for its function.

The superficial (or tangential) zone, the thinnest layer with the highest content of water, is composed by packed tightly and aligned collagen fibers parallel to the articular surface providing a smooth and congruous surface appropriate for the joint movement but, at the same time, it gives resistance to shear and tensile stresses [25]. Chondrocytes of this layer have an ellipsoid flattened form, are parallel to the joint surface and synthesize a high content of collagen, while low PGs content. The cilia are oriented away from the articular surface.

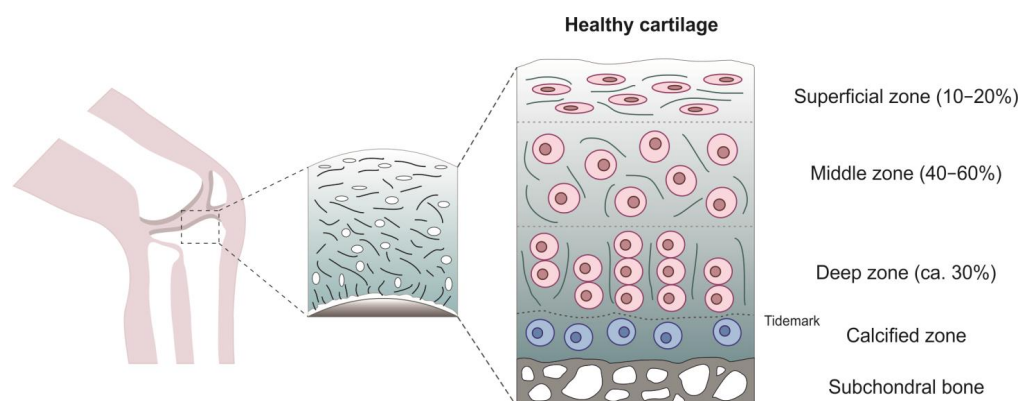


**Figure 1.** Structure of the healthy articular cartilage from the surface to the subchondral bone.

The middle (or transitional) zone is characterized by collagen fibers of larger diameter compared to that of superficial zone, organized obliquely round chondrocytes. In this zone, chondrocytes have a spheroid shape and lower density [26]. From a biomechanical point of view, this layer represents the first line of resistance to compressive forces [23].

The deep (or radial) zone contains the lowest number of spheroidal chondrocytes arranged in columnar orientation, perpendicular to the AC surface but parallel to the collagen fibers. This zone is characterized by the largest diameter of collagen fibrils and the highest concentration of PGs providing the greatest amount of resistance to compressive forces [26]. The cilium is oriented either between 2 cells or on the medial or lateral cell membrane along with the longitudinal axis parallel to the long bone [27]. The deep zone is separated from the calcified zone by the tidemark, a basophilic line of 2–5  $\mu\text{m}$  thickness [28,29]. The calcified zone anchors the cartilage to the subchondral bone and serves as a mechanical buffer between the two tissues. Chondrocytes of this zone have a hypertrophic phenotype, synthesize type X collagen and are embedded in mineralized ECM.

The fibrillar collagen network, the entrapped proteoglycan aggregates and water molecules determine the biomechanical and physical properties of AC providing tensile strength and compressive resilience based on electrostatic repulsion forces, respectively [23,30]. When AC is compressed, both water and the charged solutes are extruded from ECM, while as compression stress ends, the osmotic pressure allows PGs to reabsorb the water and the small solutes into the matrix, thus restoring the original cartilage thickness [31].

### 3. AC Pathological Changes in Osteoarthritis

AC can be affected by different diseases from rare to the most common OA [32]. OA is now considered a disease of the whole joint characterized by the involvement of all joint tissues including cartilage degeneration, subchondral bone remodeling, fibrosis and inflammation of synovial membrane, meniscal degeneration, ligaments and fibrosis and inflammation of the infrapatellar fat pad [33–37]. Obesity, diabetes, sex, genetics, joint injuries (such as meniscal damages) and aging represent risk factors associated with OA [38–40]. Currently, there is no disease-modifying therapy available for this pathology and the only option is total joint replacement for end-stage disease [41]. Inflammation and mechanopathology are both linked to OA pain, which remain one of the main problems related to the pathology that impacts on the quality of life [42,43].

During OA onset and development, AC undergoes a structural remodelling driven by many factors including mechanical stresses (wear and tear), genetic predisposition and low-grade inflammation [44–46]. Chondrocytes, which are normally quiescent cells, become active cells and acquire a hypertrophic-like phenotype resulting in an aberrant expression of inflammation-related genes and catabolic genes such as metalloproteinases [47]. The catabolic activity of chondrocytes could also be enhanced by a genetic predisposition characterized not only by alterations of different pathways (TGF- $\beta$ , Wnt/ $\beta$ -catenin, Indian Hedgehog (Ihh), Notch and fibroblast growth factor (FGF)) but also by mutations of genes linked

to ECM structure [48]. The consequence of the abnormal production of matrix-degrading enzymes is the irreversible alteration of both AC structural and functional integrity [49].

The destruction of AC is one of the pathological hallmarks in OA caused by an altered homeostasis with an increase in the catabolic state leading to proliferation, hypertrophy and apoptosis of chondrocytes, angiogenesis and calcification of cartilage and tidemark replication [25,44,47,50].

The main cellular events underlying AC destruction are ECM fibrillation and degradation secondary to mechanical breakdown and matrix metalloproteinases (MMPs) up-regulation triggering a proinflammatory cascade, collagen denaturation (especially type II collagen), decrease in elasticity, formation of crack and loss of PGs resulting in a softer ECM (Table 1) [46,47,51]. There is an increased ratio of collagen/aggrecan synthesis, a change in the composition of collagen type from collagen type II to type I, which alters the integrity of ECM networks [52].

**Table 1.** Tissue features of healthy and OA cartilage.

Point of View	Healthy Tissue	OA Tissue
Macroscopic level	Full thickness tissue Intact articular surface	Thinned tissue Eroded articular surface Patchy proteoglycan staining Increased calcified cartilage Joint space narrowing
Cellular level		
Chondrocytes	Quiescent cells	Hypertrophic-like phenotype Increased catabolism Proinflammatory proteins production Production of extracellular matrix-degrading proteinases
ECM features		
ECM Proteolysis	No	Yes
Proteoglycan content	High	Loss (proteoglycan degradation)
Collagen content	Type II and type IX collagen	Type II collagen denaturation and degradation Type X collagen production
Glycosaminoglycans	Synthesis of chondroitin sulphate, keratan sulphate and hyaluronic acid	Loss

These changes start from the superficial zone to the middle one with the formation of vertical matrix clefts and resulting in an increased AC calcification along with tidemark advancement or duplication (Figure 2) [53,54]. Therefore, AC breaks down degenerating to the subchondral bone, which results exposed in the end-stage OA [53].

OA development and progression is also supported by a chronic low-grade local and systemic inflammation through the release of cytokines and chemokines involved in chondrocytes structural and metabolic activities [48].

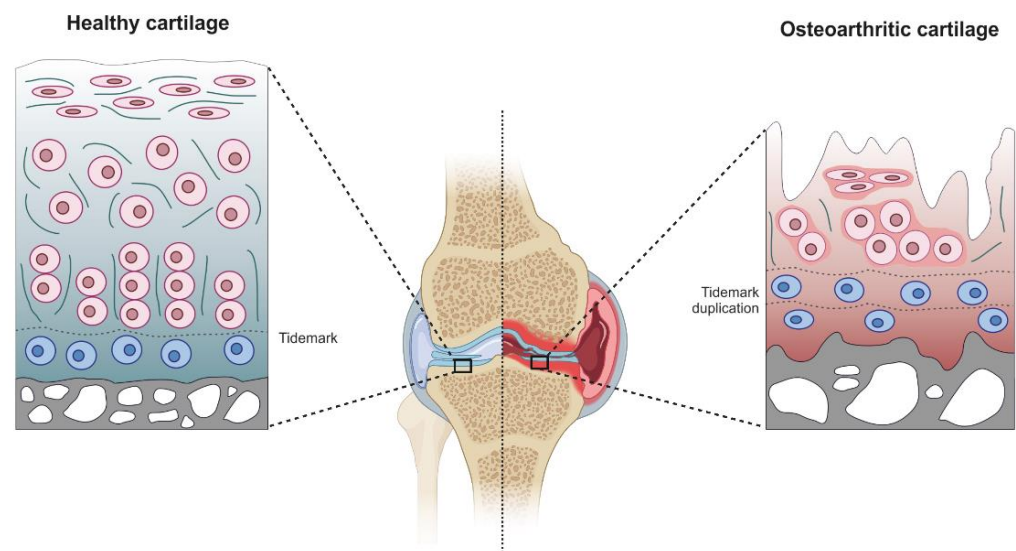


**Figure 2.** Cartilage structure in normal (left) and OA (right) tissues. In normal AC chondrocytes are diffusely distributed through ECM of AC rich in proteoglycans. A tidemark separates AC from the calcified cartilage. In OA tissue, AC appears thinned and with irregular and eroded articular surface. OA chondrocytes become hypertrophic and form clusters with increased catabolism. There is a loss of ECM and tidemark duplication. Created with [BioRender.com](https://www.biorender.com), accessed on 24 March 2023.

#### 4. Experimental Methods for the Mechanical Characterization of AC

Several experimental tests are available to characterize the mechanical properties of AC, each one allowing the identification of specific features (Figure 3), depending on the chosen setup and protocols. Experimental protocols are usually selected considering the in-vivo loading conditions, in order to simulate the effective physiological conditions and strain levels that involve AC. In particular, from the reported literature, strain levels are generally below 30%, with maximum loads depending on the joint. Independently of the adopted test, cartilage samples are usually tested in saline solution or phosphate-buffered saline (PBS), to preserve the structural integrity of the tissue and avoid the sample dehydration. Details of the analyzed studies (e.g., harvesting site, number of donors, mechanical test, etc.) on human experimental tests are reported in Table 2.

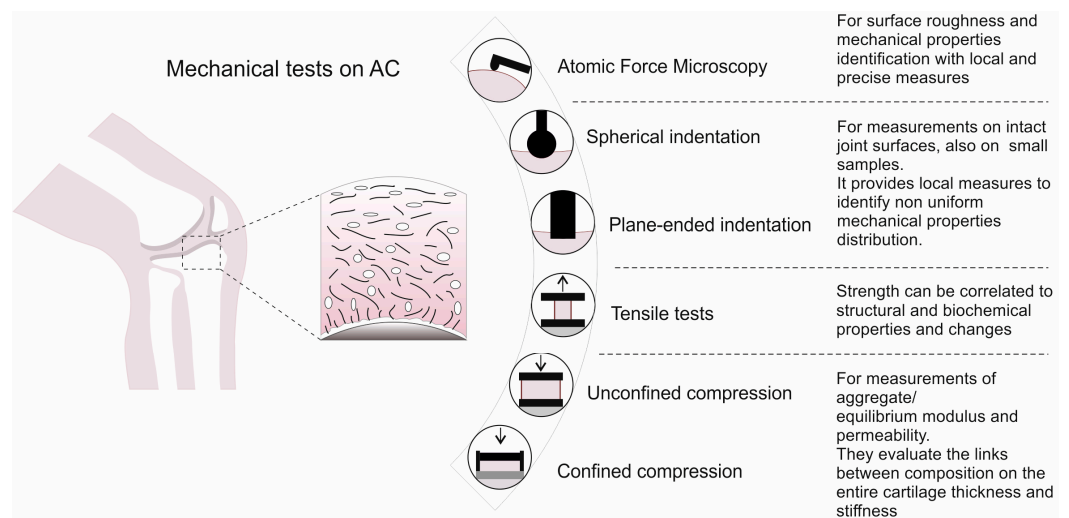


**Figure 3.** Experimental techniques that can be applied to measure the mechanical properties of AC, with a brief description of their advantages.

**Table 2.** Analyzed studies with respect to the adopted mechanical test on experimental biomechanical tests of human cartilage, harvesting site, number (sex F and M when was reported) and age of donors, if the study reported tests on healthy cartilage (H), osteoarthritis (OA) or both and adopted protocol.

Mechanical Test	Ref.	Harvesting Site	Total N of Donors	Healthy/OA	Age of the Donors (y/o)	Protocol
AFM	[12]	femoral head	50 (F:M = 25:25)	OA	40–65	N/A
	[55]	medial and lateral condyle	8 (F:M = 6:2)	OA	53–83	15 mm/s
confined compression	[56]	femoral condyle	4 (F:M = 2:2)	H	65.7	SR <sup>1</sup> displacement ramp at 0.25 um/s (60 min)
	[11]	tibia	7 (F:M = 1:6)	H and OA	68–79	4 ramps of SR, 5% strain each, (100%/s and 15 min of relaxation time)
plane-ended indentation	[57]	femoral head	16	OA	N/A	4 ramps of SR, 5% strain each, (100%/s and 15 min of relaxation time)
	[58]	metacarpal joint	12 (F:M = 6:6)	H	47–80	4 ramps of SR, 5% strain each, (2.5%/s and 5 min of relaxation time)
	[59]	patellar	6 F:M = 1:5	OA	68–79	3 ramps of SR, 5% strain each, (100%/s and 15 min of relaxation time)
	[60]	medial and lateral condyle	6 (F:M = 3:3)	OA	54–83	2 mm/s
	[61]	knee joints cartilage + subcondral bone and trabecular bone	12 (F:M = 4:8)	H and OA	31–88	500 nm amplitude (110 Hz)
spherical indentation	[62]	trapeziometacarpal joint	16 (F:M = 10:6)	H	66–101	0.1 mm at 0.5 mm/s, (relaxation time 10 s)
	[63]	lateral condyle	4 (F:M = 2:2)	H	55–61	12.5 um (1, 4 and 8 um/s)
	[9]	tibial plateau	25 (F:M = 2:1) 13 (F:M = 2:1)	OA H	72	0.3 mm at 0.1 mm/s, (10 s relaxation time)
tensile	[64]	femoral head and talus	N/A	H	7–90	0.08 mm/s
	[65]	lateral and medial condyles	31	H	30 ± 2 48 ± 1 70 ± 3	0.08 mm/s
tensile and unconfined compression	[66]	femoral head	3 1	OA H	85 ± 8 76	compression: 6 ramps of SR, 3% strain each, (0.2%/s and relaxation time 20 min. Tension: 4 ramps of SR, 2% each (0.2%/s and relaxation time 200–250 min)
	[67]	femoral condyle and femoral head	N/A	H	36–86	N/A
unconfined compression	[10]	tibia plateaus	21 (F:M = 15:6)	OA	N/A	up to 25% strain, (relaxation time 60–120 min)
	[68]	femoral head	9	OA	N/A	4 ramps of SR, 5% strain each, (100%/s and 15 min of relaxation time)
	[69]	patellar	12	H	24–78	1 ramp of SR, 10% strain, (2 mm/s and 40 min of relaxation time)
	[70]	medial and lateral condyle and tibial plateau	10 (F:M = 6:4) 3 (F:M = 2:1)	OA H	69.7 ± 9.3 59.1 ± 7.2	strain 30% with 20%/s
	[71]	femoral head	14 (F:M = 6:8)	H	63–89	100%/min up to 0.15 MPa

N/A: not available. <sup>1</sup> SR states for stress relaxation test.

#### 4.1. Atomic Force Microscopy Investigation

Atomic Force Microscopy (AFM) consists in a nanostructural imaging technique to examine sample surface (i.e., cartilage) at submicron resolution [12,72]. A basic AFM setup for biomechanical applications includes a pyramidal probe made of silicon (radius tip of about units-tens of microns [12]), or even a polystyrene or borosilicate glass sphere [73,74] set on a flexible cantilever, which is mounted on electrical piezo. During the approach phase, the sample surface interacts with the tip via Van Der Waals forces. The attractive forces

induce a deflection of the cantilever towards the sample surface. The cantilever deflection modifies the direction of the laser beam reflected from the backside of the cantilever, which enables a very accurate measurement of the deflection through an optical beam detection. AFM allows also the observation of specific structures, such as the cytoskeleton and the dynamic changes in submembranous structures [75]. AFM can be used also to measure the tribological properties of cartilage in the boundary lubricated regime [73], by applying a constant load on the cantilever tip and then measuring the surface lateral force [74]. Since AFM allows the investigation of a small scanning area [12], a rotational macrotribometer (e.g., a rheometer equipped with a tribology measuring cell) can be used for large scale measurements [73].

#### 4.2. Compression Tests

Since AC presents both a solid and a fluid phase, compression tests may be divided into two main groups: confined [56] or unconfined tests [10]. Depending on the test choice, setup and achieved results are different. Confined compression is usually performed by setting a cylindrical disc of the testing material within a confined impervious chamber with one porous plate [56]. Then, a compressive force, acting perpendicular to the plate, results in an axial fluid flow through the sample and porous plate. This test enables direct measurement of the solid matrix stiffness (the aggregate modulus,  $H_A$ ) and material permeability ( $K$ ), after a relaxation time (Zimmerman et al. [56] reported about 1 h of relaxation time to observe the equilibrium stress plateau). On the contrary, unconfined compression consists in positioning the sample between two impermeable plates, thus compressing the plates together at a certain velocity, so that the fluid exudes from the material and the sample can deform also radially [66]. This test is usually performed to achieve both instantaneous (instantaneous modulus  $IM$ ) as well as the long-term properties (equilibrium modulus  $E_{eq}$ ), after applying a constant displacement until the equilibrium is reached. Relaxation times between 15 min [68] to 120 min [10] have been reported, also depending on the different imposed strain amplitude (from 5% up to 25%, respectively). Loading protocols with 4 to 6 ramps of increasing strain amplitude of (3–5%) have been commonly adopted in stress relaxation tests in unconfined compression with the plane-ended indentation.

Moreover, dynamic tests can be performed, by applying cycles of loading-unloading at different frequencies (e.g., [76]) with the same apparatus for unconfined compression tests. In contrast with elastic materials, biological materials such as cartilage show out of phase cyclic stress and strain due to energy dissipation during the loading phase. Cycles of loading-unloading can be used to extract the dynamic elastic modulus,  $|E^*|$ , i.e., the sum of the storage modulus  $E'$  (the in-phase stress-strain relationship) and the loss modulus  $E''$  (the out-of-phase, which corresponds to the viscous component) [77].

#### 4.3. Indentation Tests

Indentation testing on cartilage shows a similar setup of the unconfined compression tests, even if one of the two plates is replaced by an indenter with a spherical or flat tip, usually smaller than the sample to test, thus enabling many points of measure on a single sample surface [9,61]. From indentation tests, the quantification of tissue/cell stiffness in terms of  $IM$  or  $E_{eq}$  is obtained, and due to material heterogeneity, results can differ one point to another, since only portions of the total samples are investigated. Indentation results can be summarized with colored maps, to highlight the variability of tissue mechanical properties within the same sample [9,62], as well as tissue degradation due to a disease such as OA. Depending on the desired stiffness properties and the sample thickness, either plane-ended or spherical-tipped indenters are appropriate. Indentation testing may be preferred when measuring cartilage stiffness on small joint surfaces when the extraction of regular samples for mechanical testing could be quite difficult and would damage the tissue [62]. In several studies from the same research group [11,57,59], the indentation testing protocol included 4 steps of increasing applied deformation (5% for each step, at 100%/s strain rate) in unconfined compression mode; each loading step was followed

by a time interval of 15 min at constant deformation to allow stress relaxation up to the equilibrium, but other protocols reported also lower relaxation time (5 min) but with lower strain rate (2.5%/s) [11,57–59], the indentation testing protocol included 4 steps of increasing applied deformation (5% for each step, at 100%/s strain rate) in unconfined compression; each loading step was followed by a time interval of 15 min at constant deformation to allow stress relaxation up to the equilibrium. Other protocols reported also lower relaxation time (5 min), but with lower strain rate (2.5%/s) [58]. For almost instantaneous measurements, indentation velocities spanned from 0.0001 mm/s [63] up to 2 mm/s [60], revealing a significant variability among the adopted protocols.

#### 4.4. Tensile Tests

As for compression and indentation tests on human cartilage, also the tensile tests have to be performed with an uncommon setup in order to keep the samples hydrated within a saline bath during the entire test durations. Rectangular sheet-like samples are obtained from AC, and then fixed from the two extremities to the machine grips, in order to apply an imposed displacement and record the force. Tensile tests are performed up to failure to characterize its fracture strength [64] or step-wise stress-relaxation tests [65,66] in order to identify instantaneous and equilibrium parameters. Lower velocities (0.08 mm/s) or strain rates (0.2%/s) were reported when performing tensile tests on human cartilage, with respect to the other tests.

#### 4.5. Friction Tests

AFM and unconfined compression tests can be used to measure also tribological properties, as stated in the previous sections. During joint activity, AC should also provide a frictionless surface to avoid high stress concentration and consequent AC wear and erosion. Generally, frictional properties between two surfaces in contact, i.e., the associated coefficient of friction (COF), depend on many factors, such as surface characteristics, roughness and anisotropy [78,79], as well as the frictional regime that characterizes the sliding (dry or lubricated friction [80]). In the case of AC, its COF may be influenced also by the test choice (i.e., rotating [81] either sliding test [82,83]), the cartilage source (e.g., both species and site), speed and duration of the test, combined with ECM subcomponents, such as GAG content [81,82]. Moreover, depending on the design of the experimental setup, different friction regimes are measured, i.e., boundary vs. mixed lubrication. When friction tests are realized on cut samples (e.g., cartilage plugs with a pin on plate setup [82,84]), it has been proved that the time to achieve the equilibrium COF linearly increases with the cartilage plug area, due to the strong influence of interstitial fluid pressurization on the cartilage COF [85]. The maintenance of a stationary contact area during the test (e.g., in the case of cartilage cylindrical plugs sliding against an impermeable surface such as metal [84]) results in an almost stationary normal pressure. Thus, the COF is initially low and then it increases due to load reassessment from the fluid to the solid matrix [84,85]. On the contrary, when a convex body is sliding on the cartilage surface, a migrating contact area is reached, which results in a migration of the contact pressure field during the sliding. This state mimics the physiological conditions within joints, with an almost constant low COF and interstitial fluid pressure (if the flow rate of the fluid within the tissue is slower than the sliding velocity) [85–87]. Under an unconfined compression test, ref. [81] measured the compressive force, torque, displacement and rotational data to calculate the torsional coefficient, while a pin-on-plate machine was realized to perform sliding test cartilage vs. cartilage, with PBS as lubricant [82], in order to obtain both static and dynamic sliding COF.

### 5. Biomechanics of Human Cartilage

Because of the biomechanical functions of hyaline cartilage in withstanding body loads, its mechanical properties represent a useful indicator of any developing diseases that may alter its functional role. Moreover, they can be correlated to imaging techniques such as Contrast-Enhanced Computed Tomography (CECT), to correlate the changes in

X-ray attenuation with alterations of ECM, e.g., glycosaminoglycan (GAG) content, which was demonstrated to be directly proportional to the cartilage compressive stiffness [88].

Cartilage can exhibit both poroelasticity and intrinsic viscoelasticity, but the contribution of the two phenomena on the time-dependent mechanical behavior is still debated [89,90]. Poroelastic flow-dependent properties are related to the rate of fluid migration within the cartilage microstructure, resulting in macroscopic mechanical relaxation, while the viscoelastic flow-independent behavior is a typical characteristic of the biological tissues, resulting from structural deformation in the network. Both may occur, depending on the strain rate, the diffusion coefficient as well as the total cartilage thickness [90]. When dynamic tests are performed on the articular cartilage, the tissue response is primarily governed by its poroelastic behavior, whereas the long-time stress relaxation states for flow-independent viscoelasticity. At the nanoscale, poroelasticity is determined primarily by aggrecans and secondarily by collagen fibrils [91].

Both confined and unconfined compression tests have been performed on human AC, in order to measure the osmotic pressure (associated by the PGs content) [56], obtain the constitutive parameters and material formulation [70], elucidate differences between biomechanics of healthy and OA AC [66], identify the contribution of the viscous damping combined with effects of proteoglycan and collagen degradation [67] and unveil elderly AC behavior during impact loading with reference to collagen, GAGs and water contents [71].

Quite surprising, since cartilage is usually compressed rather than stretched, human AC was additionally tested with tensile tests in a few studies [64–66], thus including precious insights related to the age-dependence and the origin site.

Indentation testing of human AC appeared to be the preferred method to quantify the cartilage's mechanical properties (see Table 2).

### 5.1. Influence of the Site

Samples of healthy human AC can be harvested from cadavers among different sites, such as tibia plateau, femoral head, condyles, patella and metacarpal joints. In Table 3 both  $IM$  and  $E_{eq}$  either  $H_A$  of healthy cartilage are reported.

Even if the number of studies quantifying the mechanical properties are limited, it appears that  $IM$  does not significantly vary among the articular joints, ranging from about 1 MPa for the trapezium in the metacarpal joint [62] to almost 3.5 MPa for the tibial plateau [9], with higher values when considering the instantaneous dynamic modulus during cycles of loading-unloading [11]. Dourthe et al. evaluated the trapezium and first metacarpal  $IM$  distribution via indentation (nine points for each sample) of AC from 16 fresh-frozen cadavers and observed a significant difference between the  $IM$  of the two sites, supporting the hypothesis that cartilage properties can change among the two opposing facets of the same joint. A similar finding was reported between tibial and femoral cartilage shear storage modulus by Peters et al., [61], while no consistent patterns or differences were seen at any particular site for the elastic modulus of subchondral and trabecular bone. Large variability resulted also within the same cartilage sample, as reported by Burgin et al., [71] where the  $IM$  of the different sites on femoral head (14 subjects), e.g., superior, inferior, posterior and anterior with respect to the fovea was measured. Tests of unconfined compression showed a variation between these regions, ranging from  $1.60 \pm 0.51$  MPa (inferior site) to  $2.47 \pm 0.49$  MPa (superior-anterior site). On the contrary, Seidenstuecker et al. [9] did not find a statistical difference when comparing  $IM$  of healthy cartilage from medial and lateral sites of tibial plateaus (13 subjects) obtained through indentation mapping.

**Table 3.** Mechanical properties belonging from different sites for both healthy and OA cartilage. Data are expressed as mean  $\pm$  standard deviation.

Harvesting Site	Ref.	IM (MPa) <sup>1</sup>				$H_A$ or $E_{eq}$ (MPa) <sup>2</sup>			
		Healthy	OA			Healthy	OA		
			E	M	A		E	M	A
femoral head	[12]	1.7	1.3	1.2	1.2	N/A	N/A		
	[57]	N/A	Mean $E_0$ 2 [0.1–8] Mean $E''$ 46 [2–124]			N/A	0.4 [0.02–1]		
	[68]	N/A	$E_{f0}$ OA: 0.59 $\pm$ 0.48 $E_f''$ OA: 0.61 $\pm$ 0.61 $E_{nf}$ OA: 0.23 $\pm$ 0.22			N/A	N/A		
	[71]	1.60 $\pm$ 0.51 to 2.47 $\pm$ 0.49		N/A		N/A	N/A		
condyles	[56]	N/A	N/A		0.499 $\pm$ 0.208 to 1.597 $\pm$ 0.455		N/A		
tibia plateau	[10]	N/A	N/A		N/A	0.50 $\pm$ 0.14	0.37 $\pm$ 0.13	0.28 $\pm$ 0.12	
	[11]	6.87 $\pm$ 2.57	3.69 $\pm$ 2.07	1.67 $\pm$ 1.08		1.19 $\pm$ 0.56	0.42 $\pm$ 0.25		0.21 $\pm$ 0.15
	[9]	3.43 $\pm$ 0.36	2.09 $\pm$ 0.18		N/A	N/A			
patellar joint	[69]	4.47 $\pm$ 2.22	N/A		0.53 $\pm$ 0.25				
metacarpal	[62]	MC1: 1.64 $\pm$ 1.86 trapezium: 0.99 $\pm$ 1.26	N/A		N/A	N/A			
	[58]	N/A	N/A		0.5–4		N/A		
<b>Other measurements <sup>3</sup></b>									
<b>Shear storage modulus <math>G'</math></b>									
Harvesting site	Ref.	Grade 0	Grade 0–1		Grade 1–3		Grade 0–4		
		Age < 45 y/o	45 < age < 55		55 < age < 75		Age > 75		
condyles	[61]	0.90 $\pm$ 0.55 to 1.30 $\pm$ 0.65	0.41 $\pm$ 0.54 to 0.96 $\pm$ 0.50		0.14 $\pm$ 0.31 to 0.55 $\pm$ 0.45		0.15 $\pm$ 0.09 to 0.40 $\pm$ 0.34		

E: Early; M: Moderate; A: Advanced. <sup>1</sup> When adopting a Fibril-Reinforced Biphasic Model to fit the experimental data, additional information can be obtained, such as the initial Elastic Modulus of the fibril network ( $E_{f0}$ ), the strain-dependent Elastic Modulus of the fibril network ( $E_f''$ ) and the one of the non-fibrillar matrix ( $E_{nf}$ ). <sup>2</sup> Depending on the confined or unconfined compression setup,  $H_A$  or  $E_{eq}$  can be extracted, respectively. <sup>3</sup> Cartilage shear storage modulus ( $G'$ ) was included for [61], as the results of the dynamic indentation tests.

### 5.2. Influence of the Depth

The variation in cells shape and distribution from superficial to deep cartilage, as well as collagen fibers orientation and PG content, influence the mechanical properties at the macroscale. Huttu et al. [57] observed significant positive correlations between elastic modulus and PG as well as collagen content when analyzing the entire cartilage samples thickness, while positive but not significant correlations were found when considering only the superficial cartilage (20% of the entire thickness). From the same research group [59], similar correlations were noticed also for PG content with respect to the fibril network modulus, both at 30% and 50% of the total depth. Moreover, Ihnatouski M. et al. [12] correlated the indentation depth  $h$  obtained from AFM measurements with the elastic modulus: this latter showed a maximum value of 1.7, down to 0.5 MPa when increasing  $h$  from 25 to 150 nm. On the contrary, Fischenich et al. [63] found that the mean modulus increased with increasing depth on human condyles, while the permeability decreases. However, ref. [63] in addition to the superficial zone, tested also 500  $\mu$ m below the articular surface and 500  $\mu$ m above the calcified cartilage. They found significant correlations between mechanical behavior and collagen orientation or biochemical composition when accounting for fiber orientation and depth. These strong relationships were observed for moduli with chemical composition and for permeability coefficient with respect to collagen orientation.

### 5.3. Age

Due to the limited availability of human samples, mechanical and other invasive tests are usually performed on elderly tissues (Table 2), even if the influence of ageing on the

mechanical behavior of biological tissues is well known. When dealing with human hyaline cartilage, a few studies compared the mechanical properties between subjects of different age ranges.

Kempson [64] carried out tensile tests on healthy cartilage extracted from a wide cohort of subjects with different ages, ranging between 7 and 90 y/o. Both the fracture stress and the tensile stiffness from superficial and med-depth zones of femoral head cartilage prominently decreased with increasing age, suggesting the deterioration of the cartilage structure also due to an altered metabolism of mature chondrocytes. Only a slightly and not significant decrease in the mechanical properties was observed for cartilage from the ankle joint (talus), highlighting how a different site combined with another variable i.e., ageing, could lead to different observations.

Temple et al. [92] studied the cartilage tensile properties of lateral and medial femoral condyles from three groups of young (21–39 y/o), middle (40–59 y/o) and old ( $\geq 60$  y/o) donors. Consistently with [64], results showed a decrease in the mechanical functions of the superficial zone combined with surface wear, more pronounced when moving from young to middle than from middle to old.

Moreover, Peters et al. [61] included the effects of aging (12 subjects aged 31–88 y/o) within the results obtained from dynamic indentation on both femoral condyles and tibial plateau. The cartilage properties decreased with aging, with a sharper decrease from 30 to 55 y/o, while no correlation was observed for the elastic modulus of the trabecular bone.

#### 5.4. Human vs. Animal

The difficulties in obtaining human cartilage samples prompted many authors to choose animal samples. Therefore, in the literature there are numerous experimental tests on animal specimens, and some examples are also reported for comparison with human results. The majority of the studies focused on bovine, ovine or porcine specimens (e.g., [93–96]), but others evaluated samples harvested from other species, such as equine [97], murine [98] and rabbit [99].

For each specie, different sites were investigated, usually preferring femoral condyles, tibia and patella (see Table 4 for details). As easily foreseeable, a significant variability can be observed among the species and among the anatomical sites. However, results appeared to vary between similar values, especially for bovine ( $IM$  and  $E_{eq}$  in unconfined compression, ref. [69,94], respectively) and porcine ( $H_A$  and  $E_{eq}$  in both confined and unconfined compression, [96,100]).

An interesting observation is the greater variety of performed tests on animal cartilage, such as vibrometry [94], proposed as a non-contact technique to perform dynamic mechanical tests thanks to a Laser Scanning Vibrometer, in order to measure the storage and loss moduli of cartilage. The coefficient of friction (COF) was also studied by a tribological device mounted on a two-axis load cell [101], instead of using the AFM [73].

Kotelsky et al. [98] proposed an alternative test for the measurements of elastic properties in murine cartilage, by involving computational modelling and confocal microscope-based 3D thickness mapping, thanks to the identification of cartilage deformation. This tested technique allowed authors to obtain parameters such as the Poisson's ratio  $\nu$  and elastic modulus of the solid matrix. They reported higher results if compared to others from the literature (e.g., Cao et al. [103] found 2 MPa as compressive modulus of the solid matrix and a Poisson's ratio of 0.2). However, they justified these results due to different mouse age (8–10 weeks in [98] rather than 6 months in [103]) and species, as well as different anatomical location (medial femoral condyle in [98] versus lateral tibial plateau in [103]).

**Table 4.** Representative results obtained on animal samples, useful for comparison with experimental data on human. Data are expressed as mean  $\pm$  standard deviation.

Sample Source	Ref.	Harvesting Site	Mechanical Tests	IM (MPa)	$H_A$ or $E_{eq}$ (MPa)	Other Findings
					(f [Hz]) $E_{min}-E_{max}$	
					(0.1) $14.6 \pm 6.9-$ $48.54 \pm 17.0$	
	[93]	humeral head	tensile to unconfined compression	N/A	(1) $1.16.1 \pm 5.2-$ $65.7 \pm 15.8$	N/A
					(10) $24.2 \pm 6.6-$ $61.7 \pm 13.3$	
					(40) $28.7 \pm 7.8-$ $60.9 \pm 13.4$	
Bovine	[94]	femoral condyle, trochlear groove and patella	unconfined compression, indentation and vibrometry	condyle: $1.4 \pm 0.5$ patella: $1.5 \pm 0.5$ trochlea: $1.45 \pm 0.3$	condyle: $0.48 \pm 0.12$ , patella: $0.35 \pm 0.05$ , trochlea: $0.28 \pm 0.02$	( $E_{dyn}$ ) condyle: $27.4 \pm 14.3$ patella: $46.7 \pm 11.0$ trochlea: $56.4 \pm 29.9$
	[101]	femoral condyles	wear	N/A	N/A	COF <sup>1</sup> (long) $0.265 \pm 0.033$ COF (trans) $0.247 \pm 0.034$
	[102]	tibiae	shear	N/A	N/A	shear modulus $3.16 \pm 1.01$ tangent modulus $3.29 (1.02)$ (uncompressed and compressed regions)
	[69]	patella	unconfined compression	N/A	$0.61 \pm 0.18$	N/A
Equine	[97]	medial anterior condyles	indentation	N/A	$0.6-0.9 (1)$ $0.7-0.9 (2)$	$k (mm^4/Ns) 0.004-0.019 (1)$ $k (mm^4/Ns) 0.008-0.014 (2)$
Murine	[98]	femoral condyles	custom made test	N/A	6.4	$\nu (-) 0.25$
	[103]	tibial plateau	indentation	N/A	$2 \pm 0.3$	$\nu (-) 0.2$
	[104]	patellofemoral grooves	indentation	$0.9 \pm 0.8$	N/A	N/A
Ovine	[73]	hinderleg	AFM	N/A	N/A	COF <sup>2</sup> (ddH <sub>2</sub> O) $0.3-0.33$ COF (154 mM NaCl) $0.4-0.55$ COF (2M NaCl) $0.6$ COF (synovial fluid) $0.5-0.6$
	[95]	condyles	Indentation	H $12.3 \pm 4.8$ OA $2.7 \pm 1.7$	N/A	N/A
	[96]	femurs and tibiae	Confined compression	N/A	tibia: $1.2 \pm 0.5$ femur: $0.4 \pm 0.2$	N/A
	[100]	condyles	Confined compression	N/A	tibia: H $0.5 \pm 0.1$ OA $0.4 \pm 0.2$ femur: H $0.4 \pm 0.1$ OA $0.2 \pm 0.1$	N/A
Porcine	[69]	patella	Unconfined compression	N/A	$0.85 \pm 0.25$	N/A
	[87]	mandibular condyle	Custom-built micro-tribometer and indentation	N/A	$0.25 \pm 0.06$	COF <sup>3</sup> , $0.025 \pm 0.004$ anterior-posterior sliding direction $0.028 \pm 0.004$ latero-medial sliding direction
Rabbit	[99]	mandibular condyles	AFM	$2.3 \pm 0.3$ (AM region) $1.0 \pm 0.1$ (PL region)	N/A	N/A
	[105]	mandibular condyles	AFM	neonatal $0.95 \pm 0.15$ to $1.02 \pm 0.22$	N/A	N/A
Dog	[74]	Femoral condyles	AFM	N/A	N/A	COF <sup>4</sup> , H: $0.15 \pm 0.06$ (for every load) OA: $0.22 \pm 0.09$ (load $0.5 \mu N$ ) to $0.13 \pm 0.10$ (load $5 \mu N$ )

<sup>1</sup>. Results were reported for a sliding velocity of 4 mm/s. <sup>2</sup> Results have been extracted from Figure 2C of [73], where upper limits correspond to boundary regime COF (sliding velocity of 9  $\mu m/s$ ) to mixed regime (about 120  $\mu m/s$ ). <sup>3</sup> Results refer to physiological conditions for frictional tests, by adopting a custom-built setup which allows for high interstitial pressure during the test and mimics the real joint behavior. <sup>4</sup> The authors did not report the adopted sliding velocity, but referred to boundary lubrication regime when comparing their results to other authors.

### 5.5. Tribological Properties

Contrary to the other mechanical properties, tribological properties have been reported to be location-independent [106–108], but the influence of OA is quite remarkable. Moore et al. [108] demonstrated different tribological performances due to OA, since an increase in the shear stresses was registered from the superficial zone and propagated to the deep zone, which would cause destruction of the layers through the thickness, resulting in gradual material loss.

Thanks to the fluid contribution within the solid matrix, the applied load is gradually transferred from the fluid to the soft cartilage tissue, reaching the equilibrium state. As long as the interstitial fluid is lubricating the cartilage surfaces, the friction coefficient will be maintained in a low range (about 0.001 [107]). When dynamic loading is gradually transformed to static loading, dissipating energy is mitigated by the interstitial fluid, and it permeates into the cartilage. Due to low velocities and quasi static regime, cartilage components absorb the synovial fluids, which initiate the boundary lubrication process [109]. Aging or joint disease leads to a reduction in GAG, which effectively increases the COF rate [14]. Kienle et al. [73] investigated the influence of the lubricating fluid on the friction and wear of ovine articular cartilage, both in boundary and mixed lubrication regime. They tested ddH<sub>2</sub>O, 154 mM NaCl solution (physiological concentration), 2 M NaCl solution and synovial fluid as four different lubricants. They observed an increase in the COF when increasing salt concentration at the microscale (through AFM), while a contrary trend was found with macro-friction experiments (sliding speeds > 0.1 mm/s), probably due to an ionic repulsion between the setup and the cartilage, that reduced the measured friction force. Hossain et al. [101] found no anisotropy in COF due to when testing bovine cartilage samples with applied normal load parallel or perpendicular to the collagen fibers directions on the superficial cartilage, even if GAG loss and collagen damage extended through much of the depth of the cartilage tissue, particularly for wear in the transverse direction. Few works studied the frictional properties of human cartilage; Middendorf et al. [110] evaluated the COF between human cartilage and glass through a custom-built pin-on-plate setup, and found an average value of  $0.22 \pm 0.016$ . Similarly, Li et al. [111,112] investigated the frictional behavior of AC by means of pin-on-plate friction tests in contact with different surfaces, namely cartilage, stainless steel and polyvinyl alcohol (PVA). In cyclic tests, the COF for cartilage-on-cartilage, cartilage-on-stainless steel and cartilage-on-PVA resulted equal to 0.029, 0.159 and 0.076, respectively. In all these studies, experiments were carried out with a pin-on-plate friction setup which allows for a stationary contact area during the test and thus performs the test in boundary lubrication regime (PBS as lubricant) and a vertical load was imposed to the pins in order to apply a stress of about 0.5 MPa, even though joint contact stress can reach much higher values [113]. On the contrary, physiological conditions were realized with a custom-built setup by Zimmerman et al. [87], revealing a measured COF which is one order of magnitude lower than the other reported tests, thanks to the maintenance of a migrating contact area which preserved the natural interstitial fluid pressure field and allowed for a lower friction force during the sliding (Table 4).

## 6. Influence of Osteoarthritis on Cartilage Biomechanics

The understanding and quantification of the effects of age combined with OA progression is fundamental for the prevention of the disease as well as the development of alternative solutions, such as artificial cartilage. Various mechanical alterations of a joint lead to the development of osteoarthrosis, and also imaging techniques such as CECT can be used to correlate the biochemical concentrations within the cartilage joints with the arise and progress of OA (e.g., a reduction in GAG content could be used as an indicator of early OA [114]). In Table 5 the main biomechanical alteration induced by OA are summarized qualitatively, while quantitative comparisons with healthy tissue can be found in Table 3 (human) and Table 4 (animal).

**Table 5.** Biomechanical features of healthy and OA cartilage.

Biomechanical Changes	Healthy AC	OA AC
Instantaneous and equilibrium elastic properties	Differences between anatomical sites and cartilage zones	Reduced with influence of the OA grade
Tribological properties	Low COF and efficient lubrication	COF increased at the microscale, no significant variations at the macroscale, reduced lubrication
	Smooth articular joint surfaces	Increased superficial roughness
Fibril network properties	Possible variations with cartilage depth due to different organizations	Decrease in the initial fibril network modulus from early to advanced OA, proportional to the PG content.
Permeability	Mainly governed by the physiological porosity and compressive load	Altered and increased, promoting a higher load to be transmitted to the solid cartilage component
Elastic properties of the subchondral bone	Increased with increasing age	Increased with increasing OA grade
Elastic properties of the trabecular bone	N/A	Not influenced by OA grade

Samples of OA human cartilage are mainly collected from patients who underwent total knee or hip joint replacement due to advanced OA. Indeed, the most analyzed cartilage sites are tibia plateau, femoral head and condyles. Even if various test configurations and protocols have been adopted to study the mechanical influence of OA, results were consistent and reported a decrease in all the viscoelastic properties of cartilage. In particular, Ihnatouski M. et al. [12] found decreasing average results of the  $IM$  if increasing the OA grade, from 1.7 MPa to 1.2 for both medium and advanced OA. Moreover, AFM surface mapping revealed also the changes of surface roughness when increasing OA (positive correlation) [12]. Similar results were found in unconfined compression, where  $E_{eq}$  of the cartilage decreased of about 40% from early to advanced OA [10]. Moreover, Ebrahimi, M. et al. [11] reported for the tibial plateaus a decrease in  $E_{eq}$  up to 80% with respect to the healthy tissue. Katta, J. et al. [61] observed the decrease in the shear storage modulus  $G'$  (about 70–80% of reduction), with respect to the healthy condition. From indentation tests, mechanical parameters were negatively correlated to the cell volume, due to the increase in collagen orientation angle of cartilage during the progression of OA [57]. Nissinen et al. [59] reported notable differences from early to advanced OA that resulted in a decrease in the initial fibril network modulus and the strain dependency of permeability. Increasing grade of OA was also correlated to an increase in subchondral bone, as reported by Peters et al. [61], while trabecular bone  $E$  showed no significant correlation between overall joint OA grade.

Wilusz et al. [55] realized 5 mm-thick slices of cartilage samples (healthy and OA) from femoral condyles, sectioned perpendicular to the articular surface, by adopting a cryostat microtome. These slices were used to evaluate the mechanical properties of ECM and PCM in situ through AFM indentation, testing the region between 200 and 400  $\mu\text{m}$  from the articular surface (which corresponds to middle-upper deep zone). They observed a significant decrease in the mechanical properties in both the PCM (about 30%) and ECM (about 45%) with OA when referring to the medial condyle, while no differences were found for the lateral condyle, thus rising again the strong heterogeneity of mechanical properties even within the same macroscopic sample.

Experiments on animal samples also highlighted the change in the tissue mechanical properties of OA cartilage, with respect to healthy samples [69,96,100] and a significant decrease in both the  $E_{eq}$  and  $H_A$  of porcine tibia and femur cartilage was assessed.

Indeed, healthy and pathological AC results also in a variation in the lubrication within the joint and consequently in the COF [74], an indicator for another altered function of hyaline cartilage. In particular, Desrochers et al. [74] evaluated the microscale AFM friction, revealing depth dependent changes within the few microns of the cartilage surface in early OA and an increase in the COF of about 50% for OA cartilage at the 0.5  $\mu\text{N}$  load level

with respect to healthy tissue (dog model). However, no changes were observed at higher force levels (1–5  $\mu\text{N}$ ), thus suggesting that these changes may be due to a biochemical mechanism (e.g., the reduced lubrication efficiency) and not because of roughening and softening of the surface. These observations are also supported by results at the macroscale from Caligaris et al. [115], where no differences were found in the COF when increasing OA grade.

## 7. Constitutive Modeling of Articular Cartilage

Several constitutive models have been adopted to describe the compressive behavior of AC. The most commonly used is the biphasic poroelastic model developed by Mow et al. [116], that describes the cartilage as composed of two phases: a porous solid matrix with hyperelastic properties, made of a dense network of collagen fibrils and proteoglycans with a scattered population of chondrocytes, and a fluid phase, based on the interstitial fluid (water and free ions) that can flow within the solid matrix [117]. Both the interstitial fluid and the solid matrix can be considered as almost-incompressible under physiological loading [118]. In this structure, three internal forces act within the tissue under an external load: the stress applied to the solid matrix, the pressure developed within the fluid phase and the friction between fluid and solid phases during flow, thus resulting in a time-dependent mechanical behavior [117]. Indeed, in biphasic poroelastic model, the time dependence of cartilage mechanical responses is due to the dissipative effects of the fluid phase flow.

Further generalization is proposed in poroviscoelastic models, that include flow-independent viscoelasticity in the solid-phase description, and are frequently adopted in the analysis of cartilage in confined and unconfined compression, indentation, pure shear and uniaxial tension [119–121].

The cartilage material properties considered as parameters in biphasic models are the aggregate modulus  $H_A$  and the permeability  $k$  [122]. Cartilage permeability is a complex parameter to estimate, since it varies not only with thickness, but also with the applied strain level and strain rate [123–125]. Indeed, under compressive loading in different conditions, the pore size distribution of cartilage is modified and the permeability reduced.

Lai et al. [126] proposed a triphasic cartilage model, extending the generalized biphasic models by including an ionic phase, made of negatively-charged proteoglycans. The triphasic theory has been successfully used to describe the time-dependent mechanical behavior, swelling and electro-kinetic behavior of charged hydrated articular cartilage [117]. A further insight was proposed by Huyghe and Janssen [127] with a quadriphasic model of cartilage tissue, considering cations and anions separately, in order to describe swelling more accurately. An overview about more complex multi-phasic models is given in [128].

At present, the biphasic theory is still the most popular approach for describing cartilage behavior, for several reasons. In the first place, this formulation allows to distinguish the different stress withstood by the solid and fluid phases in the tissue and this aspect may be relevant for the analysis of damage or degenerative processes of the cartilage solid component [129,130]. Then, biphasic models allow the computation of fluid flow fields within the tissue as a result of deformation, which has been used in the analysis of synovial joint lubrication mechanisms and fluid transport within cartilage [131–133].

Nonetheless, macroscopic multi-phasic models do not take into account the tissue microstructural conformation and are therefore limited in assessing the effects of microstructural differences, such as concentration and morphology variations due to subject-specific conditions or pathology. An alternative modeling approach to the above mentioned macroscopic models is the description of the cartilage mechanical response based on tissue microstructural features [134]. Examples of microstructurally based approaches include fibril-reinforced biphasic models and homogenization approaches.

Fibril-reinforced biphasic models [11,135,136] consider the different contribution of fibrillar (collagen) and non-fibrillar tissue components (a biphasic matrix made of fluid-saturated proteoglycan) and can include specific fibril arrangements. Since the fibrils

support loads in tension only, the compressive loads are sustained by the non-fibrillar component, while the tensile loads are supported by both the tissue matrix and the fibril components. The strength of this approach is modelling separately the fibrillar and nonfibrillar solid elements, highlighting their potentially different role in supporting the applied loads. Fibril-reinforced biphasic models have been also used to describe depth-dependent microstructural features [137], to include strain-dependent fibril stiffness [138] and to simulate the effects of the extracellular matrix degradation [139]. Differently, the homogenization approach, based on composite mechanics, describes the actual properties of a heterogeneous material from its constituent materials properties and their geometric configuration. Following this principle, several authors have modelled cartilage as a composite material with spheroidal inclusions, i.e., chondrocytes, embedded in an amorphous solid matrix [140,141]. This approach allows estimating the effects of modifications in chondrocyte concentration, morphology and arrangement on cartilage biomechanics. Referring to chondrocyte biomechanics, both homogeneous [142] and continuum-tensegrity models [143] have been used to study the influence of different external stimuli on the mechanical response of a single cell.

In general, microstructural models may offer further insights into the relation between mechanical behavior and structural conformation, both in healthy and OA cartilage, also envisaging possible tissue engineering strategies [144,145].

## 8. Conclusions

AC retains a fundamental mechanical function in joints biomechanics, providing an almost frictionless bearing surface and helping to distribute the loads within synovial joints. The mechanical behavior of this peculiar tissue depends on its biphasic nature, thus on both fluid and solid components, and their interaction. Due to its complex structure and behavior, its features change in time, due to aging, degenerative pathologies, injuries and so on. In particular, OA is known to be a leading cause of disability, involving changes in cartilage biomechanics during its development. In this review, we analyzed the main factors that influence the mechanical properties of AC in both healthy and disease, with a particular focus on the experimental methods and models that are currently applied within this context. The review mainly analyzed experimental results obtained from human samples highlighting the availability of a limited number of tests on human AC, among a variety of mechanical tests on animal samples. A big issue is represented by the different experimental conditions used hampering the comparison between studies. The collected information could be useful for the planning of effective experimental tests, to better unravel the differences between healthy and OA cartilage, and finally to provide an overview of the mechanical properties of different human sites that should be mimicked for future studies on artificial cartilage and tissue engineering.

**Author Contributions:** Conceptualization, E.B. and A.B.; methodology, E.B., A.B., A.P. and S.T.; validation, E.B. and A.B.; formal analysis, E.B. and A.B.; investigation, E.B., A.P., S.T. and A.B.; data curation, E.B., A.P., S.T. and A.B.; writing—original draft preparation, E.B., A.B., A.P. and S.T.; writing—review and editing, E.B., A.B., A.P., S.T., E.L.C. and P.R.; visualization, E.B. and A.B.; supervision, E.B. and A.B.; funding acquisition, E.B. and E.L.C. All authors have read and agreed to the published version of the manuscript.

**Funding:** This work was supported by MIUR, FISR 2019, Project n° FISR2019\_03221, titled CECOMES: CEntro di studi sperimentali e COmputazionali per la ModEllistica applicata alla chirurgia and by finanziamento di ateneo BIRD 2022-dotazione ordinaria ricerca (DOR) 2022 to E.B.

**Institutional Review Board Statement:** Not applicable.

**Informed Consent Statement:** Not applicable.

**Data Availability Statement:** All the analyzed works reported within this review can be found in the reference list.

**Conflicts of Interest:** The authors declare no conflict of interest.

## References

1. Patel, J.M.; Wise, B.C.; Bonnevie, E.D.; Mauck, R.L. A Systematic Review and Guide to Mechanical Testing for Articular Cartilage Tissue Engineering. *Tissue Eng. Part C Methods* **2019**, *25*, 593–608. [CrossRef]
2. Mahmood, H.; Eckold, D.; Stead, I.; Shepherd, D.E.T.; Espino, D.M.; Dearn, K.D. A Method for the Assessment of the Coefficient of Friction of Articular Cartilage and a Replacement Biomaterial. *J. Mech. Behav. Biomed. Mater.* **2020**, *103*, 103580. [CrossRef]
3. Olivetto, E.; Trisolino, G.; Belluzzi, E.; Lazzaro, A.; Strazzari, A.; Pozzuoli, A.; Cigolotti, A.; Ruggieri, P.; Evangelista, A.; Ometto, F.; et al. Macroscopic Synovial Inflammation Correlates with Symptoms and Cartilage Lesions in Patients Undergoing Arthroscopic Partial Meniscectomy: A Clinical Study. *J. Clin. Med.* **2022**, *11*, 4330. [CrossRef] [PubMed]
4. Collins, A.T.; Kulvaranon, M.L.; Cutcliffe, H.C.; Utturkar, G.M.; Smith, W.A.R.; Spritzer, C.E.; Guilak, F.; DeFrate, L.E. Obesity Alters the in Vivo Mechanical Response and Biochemical Properties of Cartilage as Measured by MRI. *Arthritis Res. Ther.* **2018**, *20*, 232. [CrossRef] [PubMed]
5. Widmyer, M.R.; Utturkar, G.M.; Leddy, H.A.; Coleman, J.L.; Spritzer, C.E.; Moorman, C.T.; DeFrate, L.E.; Guilak, F. High Body Mass Index Is Associated with Increased Diurnal Strains in the Articular Cartilage of the Knee. *Arthritis Rheum.* **2013**, *65*, 2615–2622. [CrossRef]
6. Li, Y.; Wei, X.; Zhou, J.; Wei, L. The Age-Related Changes in Cartilage and Osteoarthritis. *Biomed Res. Int.* **2013**, *2013*, 916530. [CrossRef] [PubMed]
7. Global Burden of Disease Global Burden of Disease Study 2019 (GBD 2019) Results. Osteoarthritis—Level 3 Cause. 2020. Available online: [https://www.healthdata.org/results/gbd\\_summaries/2019/osteoarthritis-level-3-cause](https://www.healthdata.org/results/gbd_summaries/2019/osteoarthritis-level-3-cause) (accessed on 1 December 2022).
8. Masson, A.O.; Krawetz, R.J. Understanding Cartilage Protection in OA and Injury: A Spectrum of Possibilities. *BMC Musculoskelet. Disord.* **2020**, *21*, 432. [CrossRef]
9. Seidenstuecker, M.; Watrinet, J.; Bernstein, A.; Suedkamp, N.P.; Latorre, S.H.; Maks, A.; Mayr, H.O. Viscoelasticity and Histology of the Human Cartilage in Healthy and Degenerated Conditions of the Knee. *J. Orthop. Surg. Res.* **2019**, *14*, 256. [CrossRef]
10. Kleeman, R.U.; Krockner, D.; Cedrano, A.; Tuischer, J.; Duda, G.N. Altered Cartilage Mechanics and Histology in Knee Osteoarthritis: Relation to Clinical Assessment (ICRS Grade). *Osteoarthr. Cartil.* **2005**, *13*, 958–963. [CrossRef]
11. Ebrahimi, M.; Ojanen, S.; Mohammadi, A.; Finnilä, M.A.; Joukainen, A.; Kröger, H.; Saarakkala, S.; Korhonen, R.K.; Tanska, P. Elastic, Viscoelastic and Fibril-Reinforced Poroelastic Material Properties of Healthy and Osteoarthritic Human Tibial Cartilage. *Ann. Biomed. Eng.* **2019**, *47*, 953–966. [CrossRef]
12. Ichnatouski, M.; Pauk, J.; Karev, D.; Karev, B. AFM-Based Method for Measurement of Normal and Osteoarthritic Human Articular Cartilage Surface Roughness. *Materials* **2020**, *13*, 2302. [CrossRef]
13. Martínez-Moreno, D.; Jiménez, G.; Gálvez-Martín, P.; Rus, G.; Marchal, J.A. Cartilage Biomechanics: A Key Factor for Osteoarthritis Regenerative Medicine. *Biochim. Biophys. Acta—Mol. Basis Dis.* **2019**, *1865*, 1067–1075. [CrossRef] [PubMed]
14. Mostakhdemin, M.; Nand, A.; Ramezani, M. Articular and Artificial Cartilage, Characteristics, Properties and Testing Approaches—A Review. *Polymers* **2021**, *13*, 2000. [CrossRef] [PubMed]
15. Bhardwaj, N.; Devi, D.; Mandal, B.B. Tissue-Engineered Cartilage: The Crossroads of Biomaterials, Cells and Stimulating Factors. *Macromol. Biosci.* **2015**, *15*, 153–182. [CrossRef]
16. Rojas-Murillo, J.A.; Simental-Mendía, M.A.; Moncada-Saucedo, N.K.; Delgado-Gonzalez, P.; Islas, J.F.; Rocho-Pérez, J.A.; Garza-Treño, E.N. Physical, Mechanical, and Biological Properties of Fibrin Scaffolds for Cartilage Repair. *Int. J. Mol. Sci.* **2022**, *23*, 9879. [CrossRef]
17. Li, M.; Sun, D.; Zhang, J.; Wang, Y.; Wei, Q.; Wang, Y. Application and Development of 3D Bioprinting in Cartilage Tissue Engineering. *Biomater. Sci.* **2022**, *10*, 5430–5458. [CrossRef] [PubMed]
18. Gu, Z.; Wang, J.; Fu, Y.; Pan, H.; He, H.; Gan, Q.; Liu, C. Smart Biomaterials for Articular Cartilage Repair and Regeneration. *Adv. Funct. Mater.* **2023**, *33*, 2212561. [CrossRef]
19. Barbon, S.; Contran, M.; Stocco, E.; Todros, S.; Macchi, V.; De Caro, R.; Porzionato, A. Enhanced Biomechanical Properties of Polyvinyl Alcohol-Based Hybrid Scaffolds for Cartilage Tissue Engineering. *Processes* **2021**, *9*, 730. [CrossRef]
20. Todros, S.; Barbon, S.; Stocco, E.; Favaron, M.; Macchi, V.; De Caro, R.; Porzionato, A.; Pavan, P.G. Time-Dependent Mechanical Behavior of Partially Oxidized Polyvinyl Alcohol Hydrogels for Tissue Engineering. *J. Mech. Behav. Biomed. Mater.* **2022**, *125*, 104966. [CrossRef]
21. Carballo, C.B.; Nakagawa, Y.; Sekiya, I.; Rodeo, S.A. Basic Science of Articular Cartilage. *Clin. Sports Med.* **2017**, *36*, 413–425. [CrossRef]
22. Gilbert, S.J.; Bonnet, C.S.; Blain, E.J. Mechanical Cues: Bidirectional Reciprocity in the Extracellular Matrix Drives Mechano-Signalling in Articular Cartilage. *Int. J. Mol. Sci.* **2021**, *22*, 13595. [CrossRef]
23. Sophia Fox, A.J.; Bedi, A.; Rodeo, S.A. The Basic Science of Articular Cartilage: Structure, Composition, and Function. *Sport. Health Multidiscip. Approach* **2009**, *1*, 461–468. [CrossRef]
24. Lu, X.L.; Mow, V.C. Biomechanics of Articular Cartilage and Determination of Material Properties. *Med. Sci. Sport. Exerc.* **2008**, *40*, 193–199. [CrossRef] [PubMed]
25. Statham, P.; Jones, E.; Jennings, L.M.; Fermor, H.L. Reproducing the Biomechanical Environment of the Chondrocyte for Cartilage Tissue Engineering. *Tissue Eng. Part B Rev.* **2022**, *28*, 405–420. [CrossRef]
26. Killen, M.-C.; Charalambous, C.P. Advances in Cartilage Restoration Techniques. In *Advances in Medical and Surgical Engineering*; Elsevier: Amsterdam, The Netherlands, 2020; pp. 71–83.

27. Yuan, X.; Yang, S. Primary Cilia and Intraflagellar Transport Proteins in Bone and Cartilage. *J. Dent. Res.* **2016**, *95*, 1341–1349. [[CrossRef](#)] [[PubMed](#)]
28. Sharma, A.; Jagga, S.; Lee, S.-S.; Nam, J.-S. Interplay between Cartilage and Subchondral Bone Contributing to Pathogenesis of Osteoarthritis. *Int. J. Mol. Sci.* **2013**, *14*, 19805–19830. [[CrossRef](#)] [[PubMed](#)]
29. Pesesse, L.; Sanchez, C.; Henrotin, Y. Osteochondral Plate Angiogenesis: A New Treatment Target in Osteoarthritis. *Jt. Bone Spine* **2011**, *78*, 144–149. [[CrossRef](#)]
30. Goldring, S.R.; Goldring, M.B. Changes in the Osteochondral Unit during Osteoarthritis: Structure, Function and Cartilage–Bone Crosstalk. *Nat. Rev. Rheumatol.* **2016**, *12*, 632–644. [[CrossRef](#)]
31. Han, E.; Chen, S.S.; Klisch, S.M.; Sah, R.L. Contribution of Proteoglycan Osmotic Swelling Pressure to the Compressive Properties of Articular Cartilage. *Biophys. J.* **2011**, *101*, 916–924. [[CrossRef](#)]
32. Krishnan, Y.; Grodzinsky, A.J. Cartilage Diseases. *Matrix Biol.* **2018**, *71–72*, 51–69. [[CrossRef](#)]
33. Martel-Pelletier, J.; Barr, A.J.; Cicuttini, F.M.; Conaghan, P.G.; Cooper, C.; Goldring, M.B.; Goldring, S.R.; Jones, G.; Teichtahl, A.J.; Pelletier, J.-P. Osteoarthritis. *Nat. Rev. Dis. Prim.* **2016**, *2*, 16072. [[CrossRef](#)]
34. Belluzzi, E.; Macchi, V.; Fontanella, C.; Carniel, E.; Olivotto, E.; Filardo, G.; Sarasin, G.; Porzionato, A.; Granzotto, M.; Pozzuoli, A.; et al. Infrapatellar Fat Pad Gene Expression and Protein Production in Patients with and without Osteoarthritis. *Int. J. Mol. Sci.* **2020**, *21*, 6016. [[CrossRef](#)] [[PubMed](#)]
35. Favero, M.; El-Hadi, H.; Belluzzi, E.; Granzotto, M.; Porzionato, A.; Sarasin, G.; Rambaldo, A.; Iacobellis, C.; Cigolotti, A.; Fontanella, C.G.; et al. Infrapatellar Fat Pad Features in Osteoarthritis: A Histopathological and Molecular Study. *Rheumatology* **2017**, *56*, 1784–1793. [[CrossRef](#)]
36. Sanchez-Lopez, E.; Coras, R.; Torres, A.; Lane, N.E.; Guma, M. Synovial Inflammation in Osteoarthritis Progression. *Nat. Rev. Rheumatol.* **2022**, *18*, 258–275. [[CrossRef](#)]
37. Englund, M.; Guermazi, A.; Lohmander, S.L. The Role of the Meniscus in Knee Osteoarthritis: A Cause or Consequence? *Radiol. Clin. N. Am.* **2009**, *47*, 703–712. [[CrossRef](#)]
38. Belluzzi, E.; El Hadi, H.; Granzotto, M.; Rossato, M.; Ramonda, R.; Macchi, V.; De Caro, R.; Vettor, R.; Favero, M. Systemic and Local Adipose Tissue in Knee Osteoarthritis. *J. Cell. Physiol.* **2017**, *232*, 1971–1978. [[CrossRef](#)] [[PubMed](#)]
39. Sowers, M.F. Epidemiology of Risk Factors for Osteoarthritis: Systemic Factors. *Curr. Opin. Rheumatol.* **2001**, *13*, 447–451. [[CrossRef](#)] [[PubMed](#)]
40. Olivotto, E.; Belluzzi, E.; Pozzuoli, A.; Cigolotti, A.; Scioni, M.; Goldring, S.R.; Goldring, M.B.; Ruggieri, P.; Ramonda, R.; Grigolo, B.; et al. Do Synovial Inflammation and Meniscal Degeneration Impact Clinical Outcomes of Patients Undergoing Arthroscopic Partial Meniscectomy? A Histological Study. *Int. J. Mol. Sci.* **2022**, *23*, 3903. [[CrossRef](#)]
41. Ghouri, A.; Conaghan, P.G. Update on Novel Pharmacological Therapies for Osteoarthritis. *Ther. Adv. Musculoskelet. Dis.* **2019**, *11*, 1759720X1986449. [[CrossRef](#)]
42. Belluzzi, E.; Stocco, E.; Pozzuoli, A.; Granzotto, M.; Porzionato, A.; Vettor, R.; De Caro, R.; Ruggieri, P.; Ramonda, R.; Rossato, M.; et al. Contribution of Infrapatellar Fat Pad and Synovial Membrane to Knee Osteoarthritis Pain. *Biomed Res. Int.* **2019**, *2019*, 6390182. [[CrossRef](#)]
43. Yu, H.; Huang, T.; Lu, W.W.; Tong, L.; Chen, D. Osteoarthritis Pain. *Int. J. Mol. Sci.* **2022**, *23*, 4642. [[CrossRef](#)] [[PubMed](#)]
44. Xiao, Z.; Su, G.; Hou, Y.; Chen, S.; Lin, D. Cartilage Degradation in Osteoarthritis: A Process of Osteochondral Remodeling Resembles the Endochondral Ossification in Growth Plate? *Med. Hypotheses* **2018**, *121*, 183–187. [[CrossRef](#)] [[PubMed](#)]
45. Loeser, R.F.; Goldring, S.R.; Scanzello, C.R.; Goldring, M.B. Osteoarthritis: A Disease of the Joint as an Organ. *Arthritis Rheum.* **2012**, *64*, 1697–1707. [[CrossRef](#)] [[PubMed](#)]
46. Torzilli, P.A.; Allen, S.N. Effect of Articular Surface Compression on Cartilage Extracellular Matrix Deformation. *J. Biomech. Eng.* **2022**, *144*, 091007. [[CrossRef](#)]
47. Goldring, M.B. Articular Cartilage Degradation in Osteoarthritis. *HSS J.* **2012**, *8*, 7–9. [[CrossRef](#)]
48. Chen, D.; Shen, J.; Zhao, W.; Wang, T.; Han, L.; Hamilton, J.L.; Im, H.-J. Osteoarthritis: Toward a Comprehensive Understanding of Pathological Mechanism. *Bone Res.* **2017**, *5*, 16044. [[CrossRef](#)]
49. Singh, P.; Marcu, K.B.; Goldring, M.B.; Otero, M. Phenotypic Instability of Chondrocytes in Osteoarthritis: On a Path to Hypertrophy. *Ann. N. Y. Acad. Sci.* **2019**, *1442*, 17–34. [[CrossRef](#)] [[PubMed](#)]
50. Kim, J.-S.; Ali, M.H.; Wydra, F.; Li, X.; Hamilton, J.L.; An, H.S.; Cs-Szabo, G.; Andrews, S.; Moric, M.; Xiao, G.; et al. Characterization of Degenerative Human Facet Joints and Facet Joint Capsular Tissues. *Osteoarthr. Cartil.* **2015**, *23*, 2242–2251. [[CrossRef](#)]
51. Liu, C.; Wang, B.; Xiao, L.; Li, Y.; Xu, L.; Zhao, Z.; Zhang, L. Protective Effects of the Pericellular Matrix of Chondrocyte on Articular Cartilage against the Development of Osteoarthritis. *Histol. Histopathol.* **2018**, *33*, 757–764. [[CrossRef](#)]
52. Maldonado, M.; Nam, J. The Role of Changes in Extracellular Matrix of Cartilage in the Presence of Inflammation on the Pathology of Osteoarthritis. *Biomed Res. Int.* **2013**, *2013*, 284873. [[CrossRef](#)]
53. Li, G.; Yin, J.; Gao, J.; Cheng, T.S.; Pavlos, N.J.; Zhang, C.; Zheng, M.H. Subchondral Bone in Osteoarthritis: Insight into Risk Factors and Microstructural Changes. *Arthritis Res. Ther.* **2013**, *15*, 223. [[CrossRef](#)] [[PubMed](#)]
54. Hodgkinson, T.; Amado, I.N.; O'Brien, F.J.; Kennedy, O.D. The Role of Mechanobiology in Bone and Cartilage Model Systems in Characterizing Initiation and Progression of Osteoarthritis. *APL Bioeng.* **2022**, *6*, 011501. [[CrossRef](#)]

55. Wilusz, R.E.; Zauscher, S.; Guilak, F. Micromechanical Mapping of Early Osteoarthritic Changes in the Pericellular Matrix of Human Articular Cartilage. *Osteoarthr. Cartil.* **2013**, *21*, 1895–1903. [[CrossRef](#)]
56. Zimmerman, B.K.; Nims, R.J.; Chen, A.; Hung, C.T.; Ateshian, G.A. Direct Osmotic Pressure Measurements in Articular Cartilage Demonstrate Nonideal and Concentration-Dependent Phenomena. *J. Biomech. Eng.* **2021**, *143*, 041007. [[CrossRef](#)] [[PubMed](#)]
57. Huttu, M.R.J.; Puhakka, J.; Mäkelä, J.T.A.; Takakubo, Y.; Tiitu, V.; Saarakkala, S.; Konttinen, Y.T.; Kiviranta, I.; Korhonen, R.K. Cell-Tissue Interactions in Osteoarthritic Human Hip Joint Articular Cartilage. *Connect. Tissue Res.* **2014**, *55*, 282–291. [[CrossRef](#)] [[PubMed](#)]
58. Lakin, B.A.; Ellis, D.J.; Shelofsky, J.S.; Freedman, J.D.; Grinstaff, M.W.; Snyder, B.D. Contrast-Enhanced CT Facilitates Rapid, Non-Destructive Assessment of Cartilage and Bone Properties of the Human Metacarpal. *Osteoarthr. Cartil.* **2015**, *23*, 2158–2166. [[CrossRef](#)]
59. Nissinen, M.T.; Hänninen, N.; Prakash, M.; Mäkelä, J.T.A.; Nissi, M.J.; Töyräs, J.; Nieminen, M.T.; Korhonen, R.K.; Tanska, P. Functional and Structural Properties of Human Patellar Articular Cartilage in Osteoarthritis. *J. Biomech.* **2021**, *126*, 110634. [[CrossRef](#)]
60. Padilla-Martinez, J.P.; Lewis, W.; Ortega-Martinez, A.; Franco, W. Intrinsic Fluorescence and Mechanical Testing of Articular Cartilage in Human Patients with Osteoarthritis. *J. Biophotonics* **2018**, *11*, e201600269. [[CrossRef](#)]
61. Peters, A.E.; Akhtar, R.; Comerford, E.J.; Bates, K.T. The Effect of Ageing and Osteoarthritis on the Mechanical Properties of Cartilage and Bone in the Human Knee Joint. *Sci. Rep.* **2018**, *8*, 5931. [[CrossRef](#)]
62. Dourthe, B.; Nickmanesh, R.; Wilson, D.R.; D’Agostino, P.; Patwa, A.N.; Grinstaff, M.W.; Snyder, B.D.; Vereecke, E. Assessment of Healthy Trapeziometacarpal Cartilage Properties Using Indentation Testing and Contrast-Enhanced Computed Tomography. *Clin. Biomech.* **2019**, *61*, 181–189. [[CrossRef](#)]
63. Fischenich, K.M.; Wahlquist, J.A.; Wilmoth, R.L.; Cai, L.; Neu, C.P.; Ferguson, V.L. Human Articular Cartilage Is Orthotropic Where Microstructure, Micromechanics, and Chemistry Vary with Depth and Split-Line Orientation. *Osteoarthr. Cartil.* **2020**, *28*, 1362–1372. [[CrossRef](#)]
64. Kempson, G.E. Age-Related Changes in the Tensile Properties of Human Articular Cartilage: A Comparative Study between the Femoral Head of the Hip Joint and the Talus of the Ankle Joint. *BBA—Gen. Subj.* **1991**, *1075*, 223–230. [[CrossRef](#)]
65. Temple-Wong, M.M.; Bae, W.C.; Chen, M.Q.; Bugbee, W.D.; Amiel, D.; Coutts, R.D.; Lotz, M.; Sah, R.L. Biomechanical, Structural, and Biochemical Indices of Degenerative and Osteoarthritic Deterioration of Adult Human Articular Cartilage of the Femoral Condyle. *Osteoarthr. Cartil.* **2009**, *17*, 1469–1476. [[CrossRef](#)] [[PubMed](#)]
66. Boschetti, F.; Peretti, G.M. Tensile and Compressive Properties of Healthy and Osteoarthritic Human Articular Cartilage. *Biorheology* **2008**, *45*, 337–344. [[CrossRef](#)] [[PubMed](#)]
67. Bader, D.L.; Kempson, G.E.; Egan, J.; Gilbey, W.; Barrett, A.J. The Effects of Selective Matrix Degradation on the Short-Term Compressive Properties of Adult Human Articular Cartilage. *BBA—Gen. Subj.* **1992**, *1116*, 147–154. [[CrossRef](#)] [[PubMed](#)]
68. Mäkelä, J.T.A.; Huttu, M.R.J.; Korhonen, R.K. Structure-Function Relationships in Osteoarthritic Human Hip Joint Articular Cartilage. *Osteoarthr. Cartil.* **2012**, *20*, 1268–1277. [[CrossRef](#)]
69. Nissi, M.J.; Rieppo, J.; Töyräs, J.; Laasanen, M.S.; Kiviranta, I.; Nieminen, M.T.; Jurvelin, J.S. Estimation of Mechanical Properties of Articular Cartilage with MRI—DGEMRIC, T2 and T1 Imaging in Different Species with Variable Stages of Maturation. *Osteoarthr. Cartil.* **2007**, *15*, 1141–1148. [[CrossRef](#)] [[PubMed](#)]
70. Robinson, D.L.; Kersh, M.E.; Walsh, N.C.; Ackland, D.C.; de Steiger, R.N.; Pandy, M.G. Mechanical Properties of Normal and Osteoarthritic Human Articular Cartilage. *J. Mech. Behav. Biomed. Mater.* **2016**, *61*, 96–109. [[CrossRef](#)] [[PubMed](#)]
71. Burgin, L.V.; Edelsten, L.; Aspden, R.M. The Mechanical and Material Properties of Elderly Human Articular Cartilage Subject to Impact and Slow Loading. *Med. Eng. Phys.* **2014**, *36*, 226–232. [[CrossRef](#)]
72. Amarouch, M.Y.; El Hilaly, J.; Mazouzi, D. AFM and FluidFM Technologies: Recent Applications in Molecular and Cellular Biology. *Scanning* **2018**, *2018*, 7801274. [[CrossRef](#)] [[PubMed](#)]
73. Kienle, S.; Boettcher, K.; Wiegand, L.; Urban, J.; Burgkart, R.; Lieleg, O.; Hugel, T. Comparison of Friction and Wear of Articular Cartilage on Different Length Scales. *J. Biomech.* **2015**, *48*, 3052–3058. [[CrossRef](#)] [[PubMed](#)]
74. Desrochers, J.; Amrein, M.W.; Matyas, J.R. Microscale Surface Friction of Articular Cartilage in Early Osteoarthritis. *J. Mech. Behav. Biomed. Mater.* **2013**, *25*, 11–22. [[CrossRef](#)]
75. Braet; Seynaeve; De Zanger; Wisse Imaging Surface and Submembranous Structures with the Atomic Force Microscope: A Study on Living Cancer Cells, Fibroblasts and Macrophages. *J. Microsc.* **1998**, *190*, 328–338. [[CrossRef](#)]
76. Park, S.; Hung, C.T.; Ateshian, G.A. Mechanical Response of Bovine Articular Cartilage under Dynamic Unconfined Compression Loading at Physiological Stress Levels. *Osteoarthr. Cartil.* **2004**, *12*, 65–73. [[CrossRef](#)] [[PubMed](#)]
77. Stolz, M.; Raiteri, R.; Daniels, A.U.; VanLandingham, M.R.; Baschong, W.; Aebi, U. Dynamic Elastic Modulus of Porcine Articular Cartilage Determined at Two Different Levels of Tissue Organization by Indentation-Type Atomic Force Microscopy. *Biophys. J.* **2004**, *86*, 3269–3283. [[CrossRef](#)] [[PubMed](#)]
78. Berardo, A.; Pugno, N.M. A Model for Hierarchical Anisotropic Friction, Adhesion and Wear. *Tribol. Int.* **2020**, *152*, 106549. [[CrossRef](#)]
79. Berardo, A.; Costagliola, G.; Ghio, S.; Boscardin, M.; Bosia, F.; Pugno, N.M. An Experimental-Numerical Study of the Adhesive Static and Dynamic Friction of Micro-Patterned Soft Polymer Surfaces. *Mater. Des.* **2019**, *181*, 107930. [[CrossRef](#)]

80. Spagni, A.; Berardo, A.; Marchetto, D.; Gualtieri, E.; Pugno, N.M.; Valeri, S. Friction of Rough Surfaces on Ice: Experiments and Modeling. *Wear* **2016**, *368–369*, 258–266. [[CrossRef](#)]
81. Lakin, B.A.; Grasso, D.J.; Shah, S.S.; Stewart, R.C.; Bansal, P.N.; Freedman, J.D.; Grinstaff, M.W.; Snyder, B.D. Cationic Agent Contrast-Enhanced Computed Tomography Imaging of Cartilage Correlates with the Compressive Modulus and Coefficient of Friction. *Osteoarthr. Cartil.* **2013**, *21*, 60–68. [[CrossRef](#)] [[PubMed](#)]
82. Katta, J.; Stapleton, T.; Ingham, E.; Jin, Z.M.; Fisher, J. The Effect of Glycosaminoglycan Depletion on the Friction and Deformation of Articular Cartilage. *Proc. Inst. Mech. Eng. Part H J. Eng. Med.* **2008**, *222*, 1–11. [[CrossRef](#)]
83. Krishnan, R.; Kopacz, M.; Ateshian, G.A. Experimental Verification of the Role of Interstitial Fluid Pressurization in Cartilage Lubrication. *J. Orthop. Res.* **2004**, *22*, 565–570. [[CrossRef](#)]
84. Forster, H.; Fisher, J. The Influence of Loading Time and Lubricant on the Friction of Articular Cartilage. *Proc. Inst. Mech. Eng. Part H J. Eng. Med.* **1996**, *210*, 109–118. [[CrossRef](#)]
85. Ateshian, G.A. The Role of Interstitial Fluid Pressurization in Articular Cartilage Lubrication. *J. Biomech.* **2009**, *42*, 1163–1176. [[CrossRef](#)] [[PubMed](#)]
86. Caligaris, M.; Ateshian, G.A. Effects of Sustained Interstitial Fluid Pressurization under Migrating Contact Area, and Boundary Lubrication by Synovial Fluid, on Cartilage Friction. *Osteoarthr. Cartil.* **2008**, *16*, 1220–1227. [[CrossRef](#)] [[PubMed](#)]
87. Zimmerman, B.K.; Bonnevie, E.D.; Park, M.; Zhou, Y.; Wang, L.; Burris, D.L.; Lu, X.L. Role of Interstitial Fluid Pressurization in TMJ Lubrication. *J. Dent. Res.* **2015**, *94*, 85–92. [[CrossRef](#)] [[PubMed](#)]
88. Lakin, B.A.; Patel, H.; Stok, K.S.; Snyder, B.D.; Grinstaff, M.W. Contrast-Enhanced Computed Tomography Imaging Using a Cationic Contrast Agent Correlates with the Equilibrium Modulus of Mouse Tibial Plateau Cartilage. *Osteoarthr. Cartil.* **2014**, *22*, S345–S346. [[CrossRef](#)]
89. Wahlquist, J.A.; DelRio, F.W.; Randolph, M.A.; Aziz, A.H.; Heveran, C.M.; Bryant, S.J.; Neu, C.P.; Ferguson, V.L. Indentation Mapping Revealed Poroelastic, but Not Viscoelastic, Properties Spanning Native Zonal Articular Cartilage. *Acta Biomater.* **2017**, *64*, 41–49. [[CrossRef](#)] [[PubMed](#)]
90. Huang, D.; Huang, Y.; Xiao, Y.; Yang, X.; Lin, H.; Feng, G.; Zhu, X.; Zhang, X. Viscoelasticity in Natural Tissues and Engineered Scaffolds for Tissue Reconstruction. *Acta Biomater.* **2019**, *97*, 74–92. [[CrossRef](#)] [[PubMed](#)]
91. Nia, H.T.; Gauci, S.J.; Azadi, M.; Hung, H.-H.; Frank, E.; Fosang, A.J.; Ortiz, C.; Grodzinsky, A.J. High-Bandwidth AFM-Based Rheology Is a Sensitive Indicator of Early Cartilage Aggrecan Degradation Relevant to Mouse Models of Osteoarthritis. *J. Biomech.* **2015**, *48*, 162–165. [[CrossRef](#)]
92. Temple, M.M.; Bae, W.C.; Chen, M.Q.; Lotz, M.; Amiel, D.; Coutts, R.D.; Sah, R.L. Age- and Site-Associated Biomechanical Weakening of Human Articular Cartilage of the Femoral Condyle. *Osteoarthr. Cartil.* **2007**, *15*, 1042–1052. [[CrossRef](#)]
93. Chahine, N.O.; Blanchette, C.; Thomas, C.B.; Lu, J.; Haudenschild, D.; Loots, G.G. Effect of Age and Cytoskeletal Elements on the Indentation-Dependent Mechanical Properties of Chondrocytes. *PLoS ONE* **2013**, *8*, e0061651. [[CrossRef](#)]
94. Espinosa, M.G.; Otarola, G.A.; Hu, J.C.; Athanasiou, K.A. Vibrometry as a Noncontact Alternative to Dynamic and Viscoelastic Mechanical Testing in Cartilage. *J. R. Soc. Interface* **2021**, *18*, 20210765. [[CrossRef](#)] [[PubMed](#)]
95. Veronesi, F.; Berni, M.; Marchiori, G.; Cassiolas, G.; Muttini, A.; Barboni, B.; Martini, L.; Fini, M.; Lopomo, N.F.; Marcacci, M.; et al. Evaluation of Cartilage Biomechanics and Knee Joint Microenvironment after Different Cell-Based Treatments in a Sheep Model of Early Osteoarthritis. *Int. Orthop.* **2021**, *45*, 427–435. [[CrossRef](#)] [[PubMed](#)]
96. Cutcliffe, H.C.; DeFrate, L.E. Comparison of Cartilage Mechanical Properties Measured During Creep and Recovery. *Sci. Rep.* **2020**, *10*, 1547. [[CrossRef](#)]
97. Reuter, T.; Hurschler, C. Comparison of Biphasic Material Properties of Equine Articular Cartilage Estimated from Stress Relaxation and Creep Indentation Tests. *Curr. Dir. Biomed. Eng.* **2021**, *7*, 363–366. [[CrossRef](#)]
98. Kotelsky, A.; Woo, C.W.; Delgadillo, L.F.; Richards, M.S.; Buckley, M.R. An Alternative Method to Characterize the Quasi-Static, Nonlinear Material Properties of Murine Articular Cartilage. *J. Biomech. Eng.* **2018**, *140*, 011007. [[CrossRef](#)]
99. Hu, K.; Radhakrishnan, P.; Patel, R.V.; Mao, J.J. Regional Structural and Viscoelastic Properties of Fibrocartilage upon Dynamic Nanoindentation of the Articular Condyle. *J. Struct. Biol.* **2001**, *136*, 46–52. [[CrossRef](#)] [[PubMed](#)]
100. Cutcliffe, H.C.; Kottamasu, P.K.; McNulty, A.L.; Goode, A.P.; Spritzer, C.E.; DeFrate, L.E. Mechanical Metrics May Show Improved Ability to Predict Osteoarthritis Compared to T1rho Mapping. *J. Biomech.* **2021**, *129*, 110771. [[CrossRef](#)] [[PubMed](#)]
101. Hossain, M.J.; Noori-Dokht, H.; Karnik, S.; Alyafei, N.; Joukar, A.; Trippel, S.B.; Wagner, D.R. Anisotropic Properties of Articular Cartilage in an Accelerated in Vitro Wear Test. *J. Mech. Behav. Biomed. Mater.* **2020**, *109*, 103834. [[CrossRef](#)]
102. Williams, J.L.; Vani, J.N.; Eick, J.D.; Petersen, E.C.; Schmidt, T.L. Shear Strength of the Pehysis Varies with Anatomic Location and Is a Function of Modulus, Inclination, and Thickness. *J. Orthop. Res.* **1999**, *17*, 214–222. [[CrossRef](#)]
103. Cao, L.; Youn, I.; Guilak, F.; Setton, L.A. Compressive Properties of Mouse Articular Cartilage Determined in a Novel Micro-Indentation Test Method and Biphasic Finite. *J. Biomech. Eng.* **2006**, *128*, 766–771. [[CrossRef](#)]
104. Boettcher, K.; Kienle, S.; Nachtsheim, J.; Burgkart, R.; Hugel, T.; Lieleg, O. The Structure and Mechanical Properties of Articular Cartilage Are Highly Resilient towards Transient Dehydration. *Acta Biomater.* **2016**, *29*, 180–187. [[CrossRef](#)]
105. Patel, R.V.; Mao, J.J. Microstructural and Elastic Properties of the Extracellular Matrices of the Superficial Zone of Neonatal Articular Cartilage by Atomic Force Microscopy. *Front. Biosci.* **2003**, *8*, 18–25. [[CrossRef](#)]
106. Katta, J.; Jin, Z.; Ingham, E.; Fisher, J. Biotribology of Articular Cartilage—A Review of the Recent Advances. *Med. Eng. Phys.* **2008**, *30*, 1349–1363. [[CrossRef](#)] [[PubMed](#)]

107. Link, J.M.; Salinas, E.Y.; Hu, J.C.; Athanasiou, K.A. The Tribology of Cartilage: Mechanisms, Experimental Techniques, and Relevance to Translational Tissue Engineering. *Clin. Biomech.* **2020**, *79*, 104880. [[CrossRef](#)]
108. Moore, A.C.; Burris, D.L. Tribological and Material Properties for Cartilage of and throughout the Bovine Stifle: Support for the Altered Joint Kinematics Hypothesis of Osteoarthritis. *Osteoarthr. Cartil.* **2015**, *23*, 161–169. [[CrossRef](#)] [[PubMed](#)]
109. Sun, Z.; Feeney, E.; Guan, Y.; Cook, S.G.; Gourdon, D.; Bonassar, L.J.; Putnam, D. Boundary Mode Lubrication of Articular Cartilage with a Biomimetic Diblock Copolymer. *Proc. Natl. Acad. Sci. USA* **2019**, *116*, 12437–12441. [[CrossRef](#)]
110. Middendorf, J.M.; Griffin, D.J.; Shortkroff, S.; Dugopolski, C.; Kennedy, S.; Siemiatkoski, J.; Cohen, I.; Bonassar, L.J. Mechanical Properties and Structure-Function Relationships of Human Chondrocyte-Seeded Cartilage Constructs after in Vitro Culture. *J. Orthop. Res. Off. Publ. Orthop. Res. Soc.* **2017**, *35*, 2298–2306. [[CrossRef](#)] [[PubMed](#)]
111. Li, F.; Su, A.Y.; Wang, A.J. Influence of Dynamic Load on Friction Behavior of Human Articular Cartilage, Stainless Steel and Polyvinyl Alcohol Hydrogel as Artificial Cartilage. *J. Mater. Sci. Mater. Med.* **2010**, *21*, 147–154. [[CrossRef](#)]
112. Li, F.; Wang, A.; Wang, C. Analysis of Friction between Articular Cartilage and Polyvinyl Alcohol Hydrogel Artificial Cartilage. *J. Mater. Sci. Mater. Med.* **2016**, *27*, 87. [[CrossRef](#)]
113. Brand, R.A. Joint Contact Stress: A Reasonable Surrogate for Biological Processes? *Iowa Orthop. J.* **2005**, *25*, 82–94.
114. Felson, D.T. Osteoarthritis: New Insights. Part 1: The Disease and Its Risk Factors. *Ann. Intern. Med.* **2000**, *133*, 635. [[CrossRef](#)]
115. Caligaris, M.; Canal, C.E.; Ahmad, C.S.; Gardner, T.R.; Ateshian, G.A. Investigation of the Frictional Response of Osteo-arthritic Human Tibiofemoral Joints and the Potential Beneficial Tribological Effect of Healthy Synovial Fluid. *Osteoarthr. Cartil.* **2009**, *17*, 1327–1332. [[CrossRef](#)]
116. Mow, V.C.; Kuei, S.C.; Lai, W.M.; Armstrong, C.G. Biphasic Creep and Stress Relaxation of Articular Cartilage in Compression: Theory and Experiments. *J. Biomech. Eng.* **1980**, *102*, 73–84. [[CrossRef](#)] [[PubMed](#)]
117. Wilson, W.; van Donkelaar, C.C.; Huyghe, J.M. A Comparison Between Mechano-Electrochemical and Biphasic Swelling Theories for Soft Hydrated Tissues. *J. Biomech. Eng.* **2005**, *127*, 158–165. [[CrossRef](#)] [[PubMed](#)]
118. Bachrach, N.M.; Mow, V.C.; Guilak, F. Incompressibility of the Solid Matrix of Articular Cartilage under High Hydrostatic Pressures. *J. Biomech.* **1998**, *31*, 445–451. [[CrossRef](#)]
119. DiSilvestro, M.R.; Suh, J.K. A Cross-Validation of the Biphasic Poroviscoelastic Model of Articular Cartilage in Unconfined Compression, Indentation, and Confined Compression. *J. Biomech.* **2001**, *34*, 519–525. [[CrossRef](#)] [[PubMed](#)]
120. DiSilvestro, M.R.; Zhu, Q.; Suh, J.K. Biphasic Poroviscoelastic Simulation of the Unconfined Compression of Articular Cartilage: II—Effect of Variable Strain Rates. *J. Biomech. Eng.* **2001**, *123*, 198–200. [[CrossRef](#)] [[PubMed](#)]
121. Huang, C.Y.; Mow, V.C.; Ateshian, G.A. The Role of Flow-Independent Viscoelasticity in the Biphasic Tensile and Compressive Responses of Articular Cartilage. *J. Biomech. Eng.* **2001**, *123*, 410–417. [[CrossRef](#)]
122. Mansour, J.M. Biomechanics of Cartilage. *Kinesiol. Mech. Pathomech. Hum. Mov.* **2003**, *2*, 66–75.
123. Mansour, J.M.; Mow, V.C. The Permeability of Articular Cartilage under Compressive Strain and at High Pressures. *J. Bone Jt. Surg. Am.* **1976**, *58*, 509–516. [[CrossRef](#)]
124. Berteau, J.-P.; Oyen, M.; Shefelbine, S.J. Permeability and Shear Modulus of Articular Cartilage in Growing Mice. *Biomech. Model. Mechanobiol.* **2016**, *15*, 205–212. [[CrossRef](#)]
125. Maroudas, A.; Bullough, P. Permeability of Articular Cartilage. *Nature* **1968**, *219*, 1260–1261. [[CrossRef](#)] [[PubMed](#)]
126. Lai, W.M.; Hou, J.S.; Mow, V.C. A Triphasic Theory for the Swelling and Deformation Behaviors of Articular Cartilage. *J. Biomech. Eng.* **1991**, *113*, 245–258. [[CrossRef](#)] [[PubMed](#)]
127. Huyghe, J.M.; Janssen, J.D. Quadriphasic Mechanics of Swelling Incompressible Porous Media. *Int. J. Eng. Sci.* **1997**, *35*, 793–802. [[CrossRef](#)]
128. Klika, V.; Gaffney, E.A.; Chen, Y.C.; Brown, C.P. An Overview of Multiphase Cartilage Mechanical Modelling and Its Role in Understanding Function and Pathology. *J. Mech. Behav. Biomed. Mater.* **2016**, *62*, 139–157. [[CrossRef](#)] [[PubMed](#)]
129. Donzelli, P.S.; Spilker, R.L.; Ateshian, G.A.; Mow, V.C. Contact Analysis of Biphasic Transversely Isotropic Cartilage Layers and Correlations with Tissue Failure. *J. Biomech.* **1999**, *32*, 1037–1047. [[CrossRef](#)] [[PubMed](#)]
130. Speirs, A.D.; Beaulé, P.E.; Ferguson, S.J.; Frei, H. Stress Distribution and Consolidation in Cartilage Constituents Is Influenced by Cyclic Loading and Osteoarthritic Degeneration. *J. Biomech.* **2014**, *47*, 2348–2353. [[CrossRef](#)]
131. Ateshian, G.A.; Wang, H.; Lai, W.M. The Role of Interstitial Fluid Pressurization and Surface Porosities on the Boundary Friction of Articular Cartilage. *J. Tribol.* **1998**, *120*, 241–248. [[CrossRef](#)]
132. Graindorge, S.; Ferrandez, W.; Jin, Z.; Ingham, E.; Grant, C.; Twigg, P.; Fisher, J. Biphasic Surface Amorphous Layer Lubrication of Articular Cartilage. *Med. Eng. Phys.* **2005**, *27*, 836–844. [[CrossRef](#)]
133. Pawaskar, S.S.; Jin, Z.M.; Fisher, J. Modelling of Fluid Support inside Articular Cartilage during Sliding. *Proc. Inst. Mech. Eng. Part J J. Eng. Tribol.* **2007**, *221*, 165–174. [[CrossRef](#)]
134. Taylor, Z.A.; Miller, K. Constitutive Modeling of Cartilaginous Tissues: A Review. *J. Appl. Biomech.* **2006**, *22*, 212–229. [[CrossRef](#)] [[PubMed](#)]
135. Fortin, M.; Soulhat, J.; Shirazi-Adl, A.; Hunziker, E.B.; Buschmann, M.D. Unconfined Compression of Articular Cartilage: Nonlinear Behavior and Comparison With a Fibril-Reinforced Biphasic Model. *J. Biomech. Eng.* **2000**, *122*, 189–195. [[CrossRef](#)] [[PubMed](#)]
136. Li, L.P.; Buschmann, M.D.; Shirazi-Adl, A. A Fibril Reinforced Nonhomogeneous Poroelastic Model for Articular Cartilage: Inhomogeneous Response in Unconfined Compression. *J. Biomech.* **2000**, *33*, 1533–1541. [[CrossRef](#)]

137. Li, L.P.; Shirazi-Adl, A.; Buschmann, M.D. Alterations in Mechanical Behaviour of Articular Cartilage Due to Changes in Depth Varying Material Properties—a Nonhomogeneous Poroelastic Model Study. *Comput. Methods Biomech. Biomed. Eng.* **2002**, *5*, 45–52. [[CrossRef](#)] [[PubMed](#)]
138. Li, L.; Soulhat, J.; Buschmann, M.; Shirazi-Adl, A. Nonlinear Analysis of Cartilage in Unconfined Ramp Compression Using a Fibril Reinforced Poroelastic Model. *Clin. Biomech.* **1999**, *14*, 673–682. [[CrossRef](#)]
139. Korhonen, R.K.; Laasanen, M.S.; Töyräs, J.; Lappalainen, R.; Helminen, H.J.; Jurvelin, J.S. Fibril Reinforced Poroelastic Model Predicts Specifically Mechanical Behavior of Normal, Proteoglycan Depleted and Collagen Degraded Articular Cartilage. *J. Biomech.* **2003**, *36*, 1373–1379. [[CrossRef](#)]
140. Wu, J.Z.; Herzog, W.; Epstein, M. Modelling of Location- and Time-Dependent Deformation of Chondrocytes during Cartilage Loading. *J. Biomech.* **1999**, *32*, 563–572. [[CrossRef](#)]
141. Federico, S.; Grillo, A.; La Rosa, G.; Giaquinta, G.; Herzog, W. A Transversely Isotropic, Transversely Homogeneous Microstructural-Statistical Model of Articular Cartilage. *J. Biomech.* **2005**, *38*, 2008–2018. [[CrossRef](#)]
142. Baaijens, F.P.T.; Trickey, W.R.; Laursen, T.A.; Guilak, F. Large Deformation Finite Element Analysis of Micropipette Aspiration to Determine the Mechanical Properties of the Chondrocyte. *Ann. Biomed. Eng.* **2005**, *33*, 494–501. [[CrossRef](#)]
143. Arduino, A.; Pettenuzzo, S.; Berardo, A.; Salomoni, V.A.; Majorana, C.; Carniel, E.L. A Continuum-Tensegrity Computational Model for Chondrocyte Biomechanics in AFM Indentation and Micropipette Aspiration. *Ann. Biomed. Eng.* **2022**, *50*, 1911–1922. [[CrossRef](#)] [[PubMed](#)]
144. Agoram, B.; Barocas, V.H. Coupled Macroscopic and Microscopic Scale Modeling of Fibrillar Tissues and Tissue Equivalents. *J. Biomech. Eng.* **2001**, *123*, 362–369. [[CrossRef](#)] [[PubMed](#)]
145. Manzano, S.; Armengol, M.; Price, A.J.; Hulley, P.A.; SGill, H.; Doblaré, M.; Hamdy Doweidar, M. Inhomogeneous Response of Articular Cartilage: A Three-Dimensional Multiphasic Heterogeneous Study. *PLoS ONE* **2016**, *11*, e0157967. [[CrossRef](#)] [[PubMed](#)]

**Disclaimer/Publisher’s Note:** The statements, opinions and data contained in all publications are solely those of the individual author(s) and contributor(s) and not of MDPI and/or the editor(s). MDPI and/or the editor(s) disclaim responsibility for any injury to people or property resulting from any ideas, methods, instructions or products referred to in the content.